Powertrain Layout and Component Design with Topology Optimization for an Electric Truck

by

Liang Deng

BEng, China University of Mining and Technology (Beijing). 2021

A Report Submitted in Partial Fulfillment of the

Requirements for the Degree of

MASTER OF MECHANICAL ENGINEERING

in the Department of Mechanical Engineering

University of Victoria

Powertrain Layout and Component Design with Topology Optimization for an Electric Truck

by

Liang Deng

BEng, China University of Mining and Technology (Beijing). 2021

Supervisory Committee

Dr. Zuomin Dong, Supervisor
Department of Mechanical Engineering

Keivan Ahmadi, Member
Department of Mechanical Engineering

Abstract

This report presents the design, optimization, and prototyping of an electric medium-duty truck (e-MDT) retrofitted from a Toyota Dyna, addressing challenges in spatial constraints, weight distribution, and structural integrity. The project focuses on developing an optimized powertrain layout, lightweight structural components, and efficient integration of electric powertrain systems to meet standard and performance requirements.

Reverse engineering was employed to create a detailed CAD model of the chassis, facilitating the analysis of spatial constraints and component placement. The powertrain layout was modelled and analyzed in terms of weight distribution and payload capacity. Structural modifications to the chassis and mounting systems were validated using finite element analysis (FEA). The motor bracket design underwent topology optimization using the Solid Isotropic Material with Penalization (SIMP) algorithm combined with hyperparameter optimization (HPO) to achieve a 48% weight reduction while maintaining structural reliability under operational loads.

The project demonstrated the effectiveness of integrating advanced computational techniques with practical engineering to overcome the challenges of vehicle electrification. Key outcomes include an optimal powertrain layout, validated structural modifications, and a lightweight motor bracket design. These contributions advance the development of sustainable, efficient, and cost-effective electric medium-duty trucks, laying the groundwork for future vehicle electrification innovations.

Keywords: Electric Medium-Duty Truck (e-MDT), Layout Design, Topology Optimization, Design of Experiments, Hyperparameter Optimization, FEA,

Acknowledgements

I would like to express my sincere gratitude to Dr. Zuomin Dong for his invaluable guidance, support, and encouragement throughout this project. His expertise and insightful advice have been instrumental in shaping the direction of this work, and his unwavering support and mentorship have greatly enriched my learning experience.

Table of Contents

List of Figures

List of Tables

1. Introduction

In 2024, the U.S. Environmental Protection Agency (EPA) introduced Phase 3 Greenhouse Gas (GHG) emissions standards, covering models from 2027 to 2032 [1]. The new rules target a substantial reduction in CO_2 emissions from trucks and buses, aiming for up to a 60% emissions reduction for vocational trucks and 40% for tractor trucks by 2032. The European regulations required truck manufacturers to reduce the average emissions of their new sales by 15% by 2025 and 30% by 2030 [2]. Also, the Emission Standard VI in China takes effect for all new heavy-duty vehicles from January 2023 for a reduction in nitrogen oxides (NO_x) and particulate matter (PM) emission limits by 70% from the previous China V standard [3].

In recent years, the sale of electrified vehicles (EVs), particularly Battery Electric Vehicles (BEV), surged as the electric drive, battery energy storage systems (BESS), and EV control technologies matured, and their costs came down quickly. However, the success is largely limited to passenger vehicles, and the electrification of heavy-duty commercial trucks has barely started. On the other hand, heavy-duty trucks are a major source of air pollution and CO_2 emissions. For instance, these trucks produce more than 70% of NO_x and 80% of PM emissions from the road fleet in China in 2022 [4]. Electrification of commercial trucks into BEV or hybrid electric vehicles (HEV) using clean fuels, based on their operation power profile and energy demand, is critical as vehicle electrification enters the next development phase.

Seeing such a demand for truck electrification, the University of Victoria's Clean Propulsion Research Team and industrial partner, Canadian Electric Vehicle, supported by the Natural Sciences and Engineering Research Council of Canada, engaged in a joint research and development project titled "Electric Medium Duty (e-MDT) Truck Design, Optimization & Prototyping." The project aims to develop e-MDT modelling, design and control optimization tools, and tests of new design methods by creating a working prototype electric truck.

The e-MDT will serve the local trade people, providing a zero-tailpipe emission solution for daily operations in the city. The e-MDT will be produced by retrofitting an old gasoline fire truck for easy production. This report documents part of the work on the e-MDT frame, chassis layout, and customized component design and topology optimization.

1.1. Medium Duty Truck (MDT) Definition and Design Challenges

Trucks are categorized by the Gross Vehicle Weight Rating (GVWR), which is the maximum allowable weight of the vehicle with a full load.

Table 1 shows the category of trucks defined by the Federal Highway Administration and U.S. EPA [1].

Table 1: Truck Category by GVWR

Gross Vehicle Weight Rating (lbs)	Federal Highway Administration	
	Vehicle Class （lbs）	GVWR Category
>6000	Class 1: < 6000	Light Duty
10000	Class 2: 6001 - 10000	
14000	Class 3: 10001 - 14000	Medium Duty
16000	Class 4: 14001-16000	
19500	Class 5: 16001-19500	
26000	Class 6: 19501-26000	
33000	Class 7: 26001-33000	Heavy Duty
> 33000	Class 8: > 33000	

The difference between the light-duty truck (LDT), medium-duty truck (MDT), and heavy-duty truck (HDT) is greater than that of GVWR in terms of design and applications. LDT and MDT commonly work in goods distribution and specific short-distance commercial use. HDTs are more often used in long-distance transportation. The commercial requirements and technical restrictions on truck range and capacity cause these differences. Most HDTs are semi-truck structures with two main components: the tractor and trailer. Multi-axles on the trailer can provide reliable axle capacity. The design challenges for e-HDT come from the working conditions. The massive payload requires large power from the motor, and long-distance transportation requires a longer range. For an 800km range e-HDT, the battery capacity would be around 1000kWh of energy, which would be over 5000kg, according to estimation [5]. Improving the massive battery pack energy density and powertrain efficiency are the critical design challenges for e-HDT. Verbruggen et al. [6] compared a multi-speed single-speed transmission for a battery-electric heavy-duty long-haul truck. The Long-Haul Driving Cycle is the driving cycle which simulates long-distance highway driving. A multi-speed transmission reduces the electric machine size by 16% and energy consumption by 1-2% without reducing top speed and acceleration performance.

However, the LDT and MDT are designed as smaller pickup trucks or cargo trucks for lower loading capacities and operation conditions, considering vehicle pass ability and turning radius. Therefore, for electric LDT and MDT, the available space for fitting in batteries is limited by the size of the vehicle, which results in more restrictions in layout design for electric LDT and MDT. For electric HDT, the battery size and layout are not as restricted by the length of the vehicle as for LDT and MDT.

To reach the required design range (180-300km) and install enough battery modules to the truck chassis, some e-MDT vehicle layouts compromise battery safety to achieve the desired mileage by locating battery modules on the outer side of the frame. Companies like Mullen Commercial [7](Mullen Three) and GreenPower Motor[8] (EV STAR truck) use this method for e-MDT truck

design to control the design cost. To overcome these spatial constraints, some companies like Ford designed the whole battery pack between the frame rails and utilized e-axle technology to make the most use of space for F-150 Lightening. Therefore, vehicle layout design is important for e-MDT due to vehicle size, range, operations, and cost restrictions.

The e-MDT studied in this work aims primarily at city road operation, carrying a working crew, and supplying materials to be used by the crew. The truck is a BEV with zero tailpipe emissions. The BESS and electric propulsion system are major components of the e-MDT. Their packaging and the accommodating truck ladder frame modifications are investigated in this work.

1.2. Battery and Its Management System

This section briefly overviews the battery and its common arrangement in a BEV.
The battery most used in electric vehicles is the lithium-ion (LIB) rechargeable battery, which uses lithium ions as the primary component for energy storage and release during charging and discharging cycles. The anode of LIB is the negative electrode made of carbon, usually graphite. The cathode of LIB is made of various materials. The material type decides some crucial characteristics of LIB, including energy density, life cycle, power density, etc.

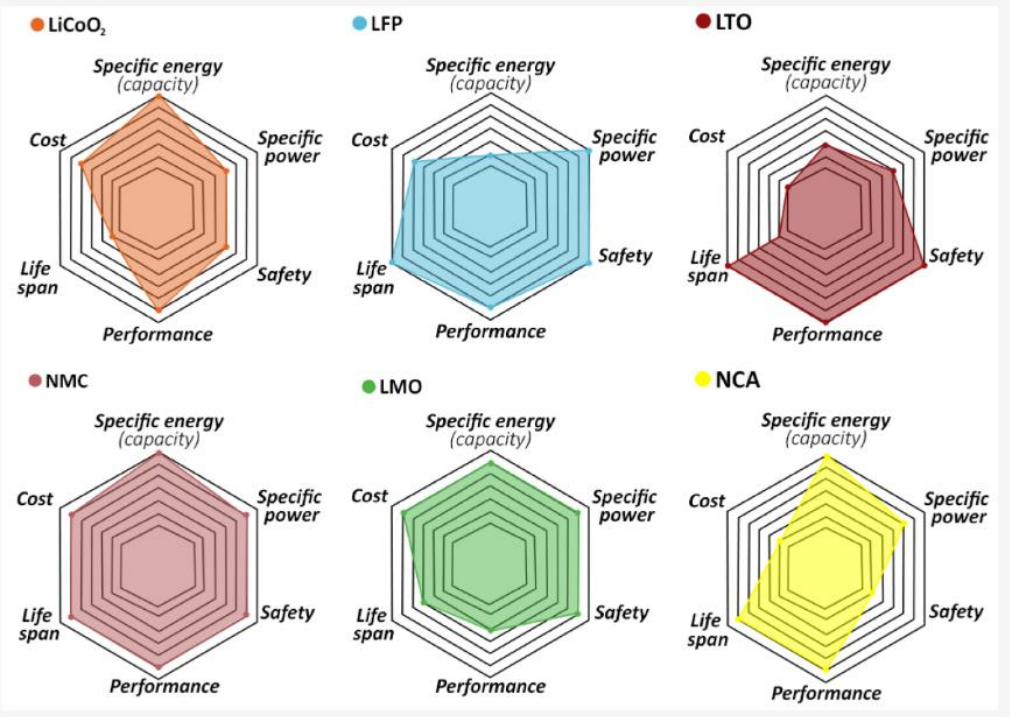

Figure 1 Comparison of Lthium-ion Batteries with Different Cathodes [9].

Commonly used LIB batteries include the lithium iron phosphate batteries and the lithium nickel manganese cobalt oxides (NMC) batteries. Figure 1 compares lithium-ion batteries with different cathodes using six metrics (features). The NMC cathode is made from a combination of nickel, manganese, and cobalt, and the LFP cathode is composed of lithium iron phosphate. These two

kinds of batteries are the most popular in the EV industry. The NMC has the highest specific energy, which means the highest energy density, and the highest specific power, which means the loading capability. The cost, however, is relatively high compared to the rest of the batteries with other cathodes. LFP has the best performance in terms of lifespan. This means the LFP battery reaches the minimum degradation level compared to others. Besides, high specific power and safety are the advantages that enable their applications in motorhomes [10] and vehicles with lower performance requirements [11], such as garbage trucks, electric road sweepers, or commercial EVs. These cells provide a high cycle life and reduced risk of thermal runaway, and have no toxic components, low internal resistance, and high-load handling capability.

The battery management system (BMS) is a critical part of the battery system. The definition of BMS varies from application to application. BMS generally refers to a management scheme that monitors, controls, and optimizes an individual's performance or multiple battery modules in an energy storage system. BMS can control the disconnection of the module(s) from the system in the event of abnormal conditions. It improves battery performance with proper safety measures within a system. A BMS is usually closely tied to the cell packaging, cooling, and thermal management.

The smallest battery unit is a cell with a certain series and parallel structure. For example, cells of the Nissan Leaf battery (s96p2) are packaged in a structure of 96 series cells and two parallel modules, as indicated by "s96p2". In a conventional packing design, only 25%-30% of the volume is battery material[12] For the ease of battery pack design and production, traditional small batch EV production often uses standard battery modules to form the pack, as shown in Figure 2 (left). These modules consist of battery cells in series and parallel and provide 40-48V output.

Reducing the inactive fraction of a battery pack is important to improve battery energy density. The "Cell-to-Pack" (CTP) technology is developed to make the most utilization of the interior of the battery and optimize the structure of the battery pack (Figure 2). One of the developers of CTP, the Chinese company CATL [12], reports that 15 %–20 % more storage material is housed in the same assembly and at the same time, 40 % fewer parts are required for production. CATL released that their third-generation CTP battery increases the LFP pack energy density to around 85% of a conventional NMC811 battery [13]. For example, the battery pack for the Tesla Model S contains 16 modules with 12 cells, while the new Model 3 pack with the CATL battery contains only four modules, as shown in Figure 3.

Compared with traditional battery packs currently available on the market, the volume utilization rate of CTP battery packs has been improved by 15%–20%, the number of components reduced by 40%, and the production efficiency increased by 50% [12]. The development of CTP technology is the main reason for the resurgence of LFP, which compensates for the LFP's lack of energy density. In addition, the cost advantage of LFP in a high commodity price market is one reason for the resurgence. Although CTP improves energy density over traditional battery pack design, the design of CTP will significantly change the frame design. In our e-MDT prototype, we followed

the conventional battery pack design approach using battery modules rather than individual cells to reduce pack design complexity and development time since we tried to reuse the existing frame.

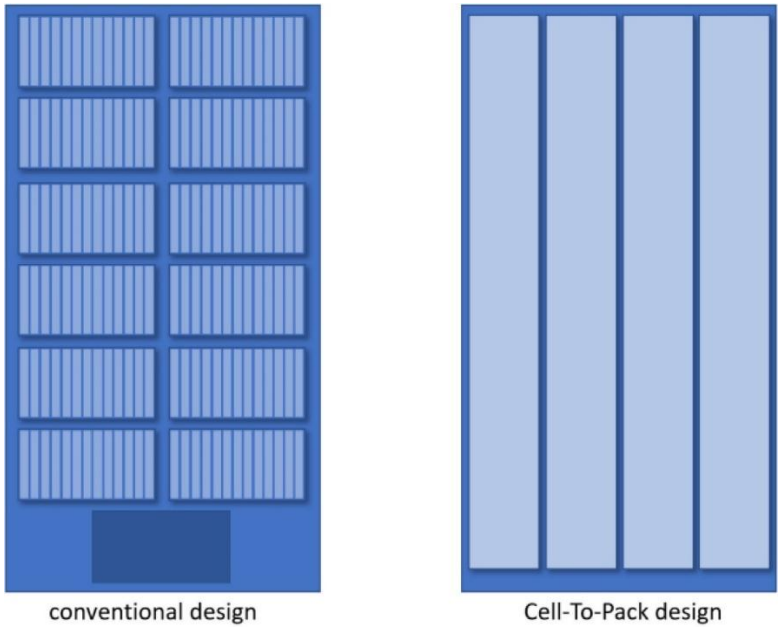

Figure 2: Conventional Pack vs Cell-to-Pack [12]

1.3. Prototype of e-MDT

The project aims to design an e-MDT and build a prototype by converting the 1999 Toyota Dyna truck shown in Figure 3. Dyna is a double cabin medium-duty truck with a 4550 kg (10,031lbs) GVWR.

Figure 3: Picture of the Prototype Dyna.

The prototype e-MDT is converted from this truck by replacing the conventional powertrain. The design requirements for the prototype are illustrated in Table 2. Powertrain component selection is based on the requirements. The main components are the motor, gearbox, driveshaft, and battery pack, designed with a required number of modules and a thermal management system.

Retrofitting traditional internal combustion engine (ICE) truck frames for electric powertrain systems presents significant challenges. The conventional frame of Dyna, designed for diesel engine drivetrain components, lacks the spatial and structural accommodations necessary for electric powertrain elements, such as motors, battery packs, and cooling systems. Modifications to the frame should be designed and analyzed to ensure sufficient structural stiffness to accommodate the e-powertrain layout.

Weight distribution is critical for ensuring the safety and performance of electrified medium-duty trucks. Positioning heavy components, such as battery packs and the motor, directly affects the vehicle's center of gravity, axle loads, and overall dynamics, including handling and braking performance. An e-MDT design must adhere to regulatory requirements, ensuring the front axle carries at least 30% of the Gross Vehicle Mass (GVM) for stability during operation.

Table 2: Prototype e-MDT Design Requirements

Performance	Design Requirement
Top Speed (Loaded)	110 km/hrs
Acceleration	0-55 km/hrs in 10s
Range	200-300 km
Gradeability	< 25
Charge Time	2 hrs (80% SoC; Fast) 6 hrs (100% SoC; Slow)
Peak Power	180 kW
Peak Torque	1200 Nm
Battery Capacity	120 kWh

In our prototype development, reverse engineering played a pivotal role in developing the CAD model of the Toyota Dyna chassis. Detailed frame, axles, and cabin underside measurements were manually taken and verified against collected 2D drawings. This process enabled the identification of feasible spatial configurations and provided a foundation for the precise integration of powertrain components, ensuring compatibility with the modified frame structure.

1.4. Objectives

As part of the e-MDT design project, this report documents the powertrain layout and comparison, customized component design and analysis, and the potential of applying topology optimization for vehicle weight reduction.

- To optimize the powertrain layout for an electric medium-duty truck (e-MDT) by addressing spatial constraints, weight distribution, and regulatory requirements.
- To design and analyze structural modifications to the chassis and mounting components using finite element analysis (FEA) to ensure safety and performance under operational loads.
- To apply topology optimization, enhanced by hyperparameter optimization (HPO), to reduce the weight of critical components, such as the motor bracket to ensure structural integrity.
- To explore the integration of advanced computational tools and practical engineering solutions for sustainable and efficient vehicle electrification.

1.5. Structure of the Report

This report is organized into six chapters. Chapter 1 provides an overview of the need for electrification of medium-duty trucks (e-MDTs) and outlines the project objectives and challenges, including spatial constraints, payload limitations, and regulatory requirements.

Chapter 2 focuses on the development and evaluation of the e-MDT powertrain layout. It covers the selection of powertrain components, the chassis's reverse engineering, and the assessment of layout options based on spatial and dynamic constraints.

Chapter 3 details the structural design and analysis of key components, including the gearbox mounting bracket and frame modifications. Finite element analysis (FEA) ensures structural integrity under static and fluctuating operational loads.

Chapter 4 introduces the topology optimization process using the Solid Isotropic Material with Penalization (SIMP) algorithm. Hyperparameter optimization (HPO) is applied to refine algorithm parameters to achieve optimal material distribution for the motor bracket design.

Chapter 5 describes the application of topology and hyperparameter optimization to design a lightweight motor bracket. The optimized design is validated through FEA for static and fatigue performance.

Chapter 6 summarizes the findings and technical contributions of the project, highlighting the benefits of applying advanced optimization techniques. It also suggests potential areas for further research.

2. Powertrain Layout Design

The powertrain system of the e-MDT was first modelled based on the truck's technical specifications and operation profile. Using the constructed MATLAB/Simulink model, the performance and limitations of various powertrain designs are investigated. The powertrain system design optimization using this Model Based Design (MBD) method was carried out to identify the optimal sizes of the propulsion motor, gear reduction and BESS. The best fit commercially available propulsion motor/controller and gear reduction transmission are selected. Similarly, with several battery packs of selected battery modules, the BESS is designed to include the battery modules in series and parallel with proper cooling plates, coolant manifolds, connecting pipes, structure elements, and a battery management system (BMS). The separated packs allow adequate weight distribution and structure integrity within the ladder frame. The team did these before the powertrain layout design.

The e-MDT powertrain layout design creates accurate CAD models of the selected components and the truck's chassis. The truck frame and cab geometry and sizes are captured by measurement and using a laser scanner. These accurate geometric models define the available space and spatial constraints to set the stage for powertrain component placement. Layout constraints are analyzed to guide design decisions, including frame modifications and attaching mechanism design. The truck's weight distribution and departure angles are also obtained for design improvements.

Three layout options are evaluated for feasibility, safety, and performance, with the optimal layout selected based on both structural and dynamic considerations. The chapter concludes with weight distribution and load capacity analyses, establishing a foundation for the structural modifications discussed in the next chapter.

2.1. Overview of e-MDT Prototype Design

The detailed vehicle dynamics, powertrain system models, and the standard vehicle drive cycle, such as the Urban Dynamometer Driving Schedule (UDDS), form the Software-in-Loop (SIL) vehicle performance and energy efficiency evaluation platform. The vehicle model provided key outputs, including energy consumption, maximum vehicle range, and powertrain operating conditions, such as torque requirements. The powertrain components and system were modelled and simulated using MATLAB/Simulink.

Due to the limited availability of experimental data for electric machines, a Permanent Magnet Synchronous Motor (PMSM) was scaled to meet manufacturer specifications in the simulation. Additional considerations, such as cost comparisons across suppliers and low-volume supply availability, informed the selection of components. The iM-225 motor, supplied by Cascadia Motion, and the Mid-Series Sigma Gearbox were chosen. The motor has a mass of 64 kg, while the gearbox weighs 45 kg. The motor delivers a peak output torque of 500 Nm.

The energy storage system (ESS) utilizes 1p12s EP-LFP battery modules supplied by EcoPower Limited, China. Due to the maximum voltage limitation of the iM-225 motor, the number of modules is restricted to 10, resulting in a total ESS capacity of 102.16 kWh. Simulation results from the SIL configuration indicated a travel range of 308 km and an energy efficiency of 26.5 kWh/100 km. The ESS size emerged as a critical constraint in the layout design.

2.2. e-MDT CAD Model Preparation

The retrofitting process involves integrating 10 battery modules, an iM-225 motor, and a Mid-Series Sigma gearbox into the chassis of a Toyota Dyna. The primary challenge is determining the spatial orientation of the original Dyna chassis's battery modules and powertrain components.

A CAD chassis model was created using a reverse engineering approach, ensuring an accurate representation of the feasible design space. Critical dimensions of the main components, including the ladder frame, front and rear axles, and cross members, were measured manually. The Dyan truck chassis is verified as KDY230L-PBMEYW3. The measurements were subsequently cross-verified with 2D drawings, as detailed in Appendix A, to ensure precision and compatibility.

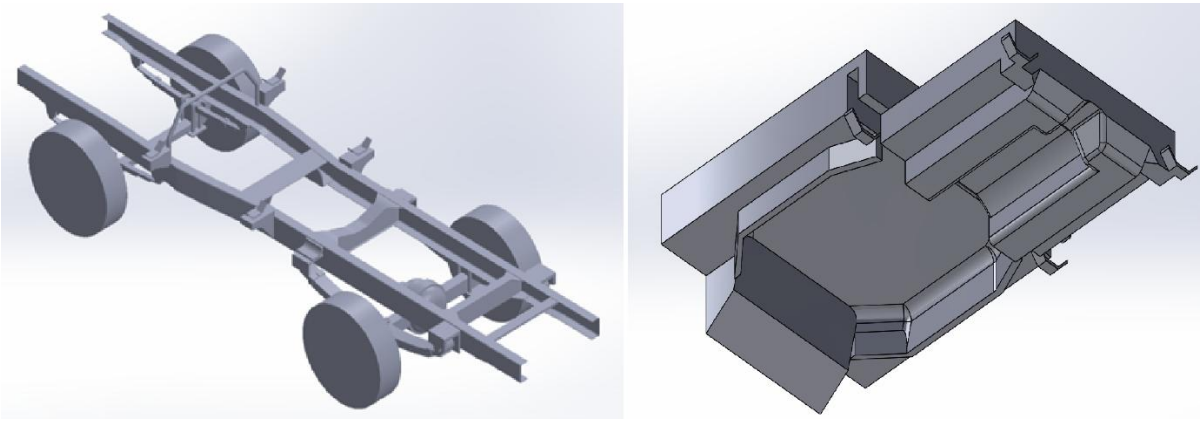

Figure 4: Dyna Frame (left) and Cabin under Surface (right) CAD Model

The CAD models of the frame and the underside of the Cabin were developed using SolidWorks, as illustrated in Figure 4. Detailed measurements of the Cabin's underside dimensions and geometry scan results are provided in Appendix SIMPA. To ensure accurate positioning of the cabin surface, the mounting structure details were measured with high precision. These measurements also serve as critical references for defining cabin loading positions in subsequent frame loading analyses.

2.2.1. Layout Design Constraints

The layout design significantly impacts the truck's weight distribution, which is crucial for evaluating axle loads and overall vehicle dynamics, including braking, handling, and gradability performance. Additionally, the truck's center of gravity (COG) directly influences the load ratings of the front and rear axles.

When fully loaded, the Toyota Dyna's Gross Vehicle Mass (GVM) is 4,350 kg. According to the design constraints, the front axle must bear at least 30% of the GVM, resulting in a minimum front axle load of 1305 kg, as calculated using Equation (1). The Dyna model KDY230L-PBMEYW3 specifies a front axle capacity of 1800 kg and a rear axle capacity of 2550 kg.[14] These specifications establish the design and operational limits for the vehicle.

$$\frac{Front\ Axle\ Mass}{Gross\ Vehicle\ Mass} \times 100\% \geq 30\% \quad (1)$$

Using the CAD models generated through reverse engineering, spatial constraints were identified as the primary limitation for the layout design. The frame's rear section has a width of 607 mm, restricting the maximum number of battery modules to three that can be arranged laterally between the two frame members. Additionally, a clearance of 35 mm is maintained on each side of the frame.

The design requires a departure angle of at least 20 degrees. As illustrated in Figure 5, the departure angle is the angle formed between the ground and the lowest point at the rear of the vehicle. The departure angle for a configuration with two rows of modules is 11.98 degrees, below the design requirement. Consequently, the battery pack in the rear section must adopt a 3x1 pattern to meet the departure angle criteria.

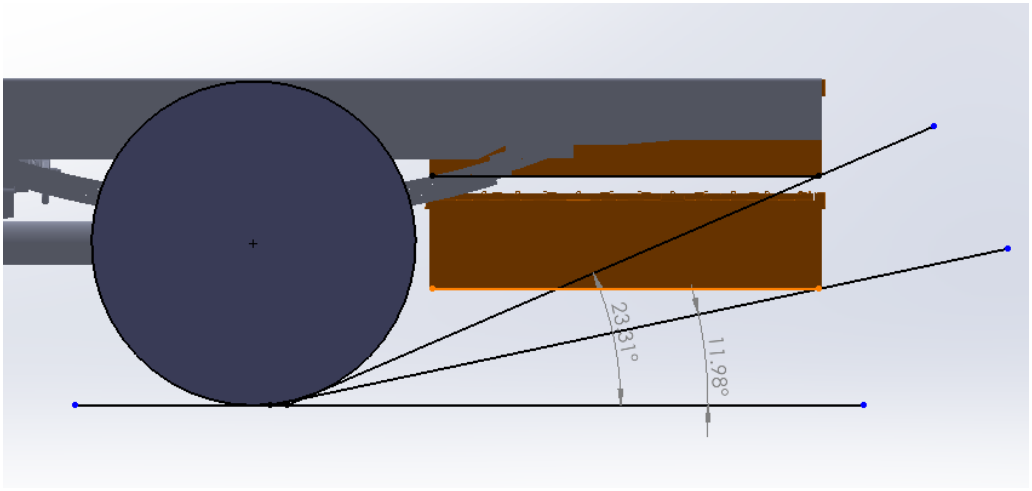

Figure 5: Departure Angel Measurement

2.2.2. Layout Generation

Three potential powertrain component layout designs were developed based on the constraints outlined in the previous section. The first approach, illustrated in Figure 6, involves placing seven battery modules symmetrically under the Cabin in a 3x1 and 4x1 pattern. This layout preserves most available space between the frame members and provides flexibility for the gearbox and motor assembly. Additionally, it retains most of the structural features of the prototype vehicle frame.

However, this design presents a notable limitation: the clearance between the side surface of the modules in the second row and the frame edge is only 10 mm on each side. This minimal clearance poses challenges due to potential measurement errors in the CAD model and the complexity of designing battery enclosures. As a result, significant additional work would be required to implement this layout effectively.

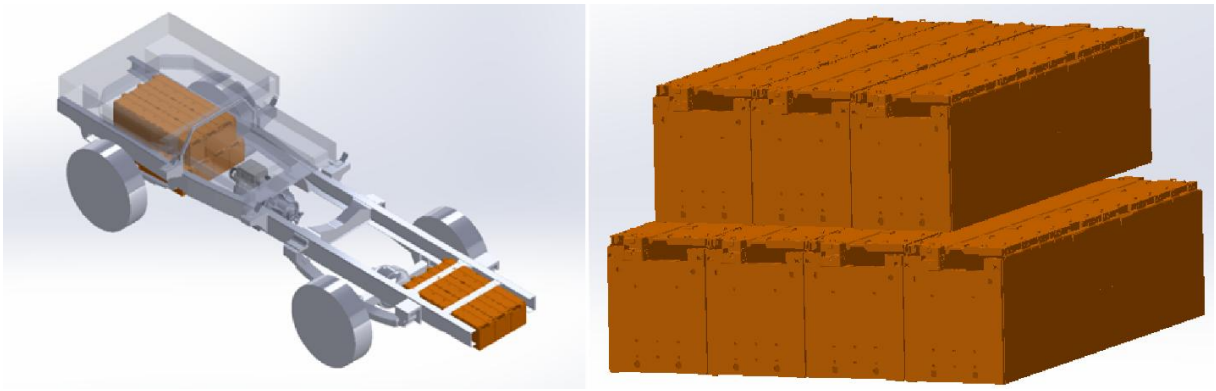

Figure 6: Layout Design One (Left) and Battery Module Pattern under the Cabin(right)

The number of modules in the front pack was reduced to three, while the remaining four modules were positioned on each side of the frame between the wheels, as shown in Figure 7, to address the clearance issue in the front. This layout increases the clearance to 94 mm on each side, providing sufficient space for the battery pack enclosure design. Additionally, the single-row configuration of modules eliminates interference with the cabin structure.

However, this layout has notable disadvantages. Placing batteries on the sides exposes them to damage from road debris. The battery enclosures are also at higher risk of encountering splash and flooding, which increases the likelihood of water intrusion into the housing. These factors could compromise the durability and safety of the battery system.

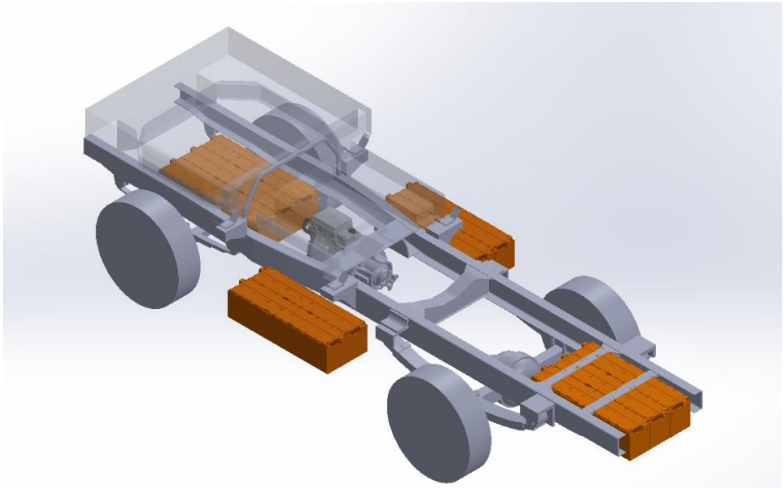

Figure 7: Layout Design Two

The battery layout was adjusted to accommodate four modules, as shown in Figure 8, to maximize the usable design space under the Cabin. Once more detailed scan data of the Cabin's underside was obtained, this configuration was validated, confirming no interference with other components on the frame. A 3x1 pack was also positioned behind the front battery pack, following a design similar to the rear pack's. This approach optimizes spatial efficiency while maintaining compatibility with the overall vehicle structure.

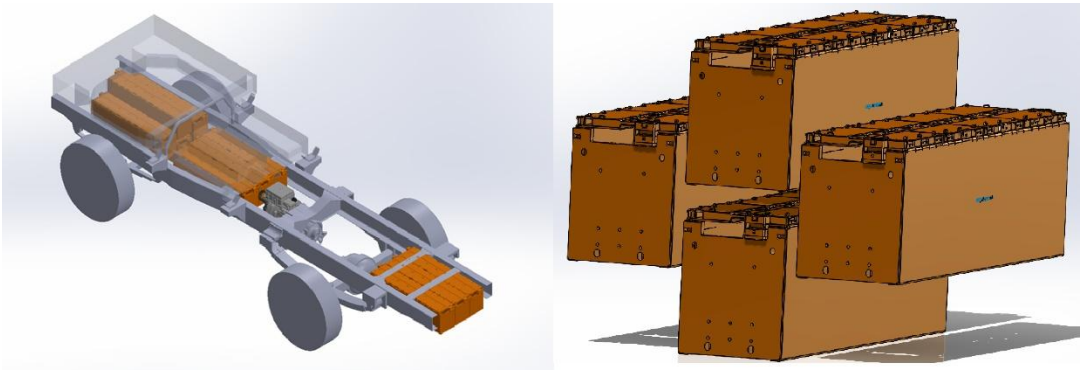

Figure 8: Layout Design Three (left) and Battery Module Pattern under the Cabin (right)

2.2.3. Weight Distribution and Load Capacity Calculations

For the prototype vehicle, many components have unknown weights and undefined positions, making it challenging to estimate weight distribution accurately using the CAD model developed for spatial orientation design. The prototype vehicle, a Toyota Dyna, was disassembled to provide baseline weight information, and unnecessary components were removed. This baseline data enables a longitudinal calculation of the vehicle's weight distribution. The CAD model with assigned weight information exhibited a 10% difference from the test results. The CAD models were calibrated based on the test data to improve accuracy. The Dyna removed powertrain weighs 1774.5 kg and 1083 kg on the front and rear axle. The weights and positions of the electric powertrain components were determined using specifications and manufacturer manuals, ensuring accurate input for subsequent design and analysis. The calculations of the center of gravity and payload could be derived as below:

$$d_{COG} = \frac{\sum_{i=1}^{n} d_i \, m_i}{m_{total}} \tag{2}$$

$$L_{front} = \frac{(D_{wb} - d_{COG}) \, m_{total}}{D_{wb}} + m_{front} \tag{3}$$

$$L_{rear} = \frac{d_{COG} \, m_{total}}{D_{wb}} + m_{rear} \tag{4}$$

$$m_{payload} = \begin{cases} L_{rmax} - L_{rear} & if\left(L_{front} + L_{rmax} < m_{register}\right) \\ m_{register} - L_{front} - L_{rear} & if\left(L_{front} + L_{rmax} > m_{register}\right) \end{cases} \quad (5)$$

where d_{COG} is the distance of the center of gravity to the front axle; d_i and m_i are the distances for each electric powertrain component to the front axle and mass; m_{total} is the sum of component mass; L_{front} and L_{rear} are the front and back axle loads; D_{wb} is the wheelbase; m_{front} and m_{rear} are mass of the empty dyna distributed on the front and rear axle; $m_{payload}$ is the payload capacity; L_{rmax} indicates the rear axle capacity; $m_{register}$ is the weight registered in ICBC for the electrified Dyna.

Table 3: Crucial Components in Dyna Electrification

Component	m_i (kg)	d_i (mm)
Chiller	30	1014
Cab Hydraulic Lift	10	565
Truck Bed	24	2946
Power Pack for Lift	60	3742
Motor & Gearbox	102	2160
full loaded passengers	300	764

The registered weight and rear axle load capacity are the main constraints on the truck's payload. The rear axle is assumed to reach the limit to get as much payload capacity as possible. The weight distribution results for layouts two and three are shown in Table 4 below.

Table 4: Load Calculation for Layouts 2 and 3

	Front Axle Load (kg)	Payload (kg)	Rear Axle Load (kg)	Front Axle Rate
Layout Option 2	1780	1062	2550	41.1%
Layout Option 3	1834	1067	2455	42.8%

The front axle rate for both layouts exceeds the 30% threshold, and the payload capacity for each layout surpasses 1000 kg. However, the axle load analysis reveals that the suspension strength of the original Toyota Dyna is insufficient for layout option three, as it exceeds the rear axle capacity by 34 kg. The ideal weight distribution for the newly designed layout targets 30% of the Gross Vehicle Weight (GVW) on the front axle, aligning with previous standards to ensure optimal handling and braking performance. In this design, the empty truck naturally has a front axle load exceeding 30% without the payload. However, the front axle distribution is also constrained by its

maximum load capacity. These two factors—maintaining stability while under axle load limits—are the primary considerations in the weight distribution analysis.

While this design is common in many converted commercial trucks due to its minimal frame modifications and efficient use of chassis space, layout option two is still unsuitable for the final design. According to the Federal Motor Vehicle Safety Standards (FMVSS) in the United States, Note 305 specifies that “batteries cannot be positioned where they are likely to deform significantly during collisions (crush zones).” The side-mounted battery packs in layout option two falls within the crush zone during side impacts, posing safety risks.

Layout option three provides significant advantages. All ten battery modules are securely housed within the frame area, and the middle battery pack aligns with the vertical level of the original drivetrain components. This configuration has enough vehicle ground clearance. However, this layout compresses the gearbox and motor area, leaving insufficient longitudinal space for the powertrain assembly.

After evaluation, the project team selected layout option three as the most feasible solution for the productive e-MDT truck design. This layout necessitates reinforcement of the prototype vehicle's front axle and frame extension, as discussed in the following sections. Additionally, the placement of battery modules within the ladder frame interferes with the cross-members, requiring a redesign of the frame to incorporate new cross-members and accommodate the updated loading conditions, which will be discussed in Chapter 3.

2.2.4. Summary

This chapter outlines the methodologies and constraints influencing the layout design and evaluates multiple configuration options.

The initial CAD model of the chassis was developed through reverse engineering to identify feasible spatial orientations for the components. Key design constraints, such as frame width, departure angle, and weight distribution, were analyzed to guide the placement of the battery modules. The final layout was determined by evaluating the two competing layout options' weight distribution and axle loads. Layout option three was chosen as the final layout.

This chapter establishes the foundation for integrating powertrain components, addressing both spatial and structural challenges, and paves the way for detailed frame redesign and analysis in later chapters.

3. e-MDT Powertrain Component Design

The e-MDT powertrain includes three customize-designed components, i.e., the gearbox mounting bracket, frame, and motor bracket design. In this chapter, the first two components will be described in detail. The motor bracket design will be explained in Chapter 5 since this task involves topology optimization and hyperparameter optimization.

3.1. Gearbox Mounting Bracket Design and Analysis

3.1.1. Gearbox Mounting Components Design

The gearbox mounting components include a crossbar and a mounting plate. The crossbar is made by a T-shaped beam bolted on the frame's inner surface. The mounting plate assembly between the gearbox and crossbar is shown in Figure 9. The mounting components are restricted to sheet metals for ease of fabrication. To save cost from ordering raw materials, the crossbar and mounting plate are of the same thickness, 0.25 inch, in the same 4130 Steel.

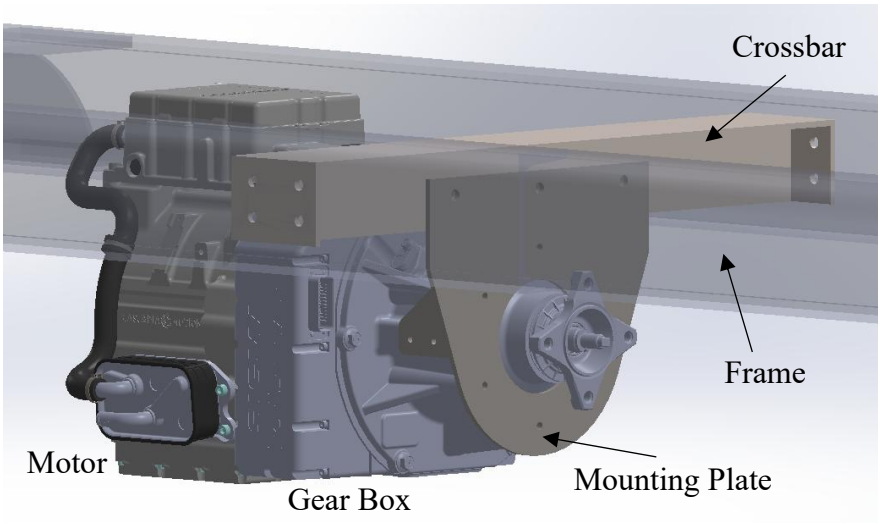

Figure 9: Gearbox Mounting Assembly

The size of mounting holes on the frame to the crossbar is calculated with 20G lateral deceleration. The material of bolts between the frame and crossbar is designed to be grade 8. The bolt size is estimated by calculating the maximum allowed shear stress with the designed number of bolts on each bracket shown in Appendix B. The size of bolts is designed to be M10 in a conservative way. Before determining the hole size on the crossbar for securing the mounting plate, it is essential to calculate the weight distribution on the motor and gearbox mount. The motor and gearbox assembly's center of gravity (COG) is obtained from the explicit CAD model provided by vendors Cascadia Motion and Sigma Powertrain, respectively. As shown in Appendix C, the COG of the assembly is 220.4mm to the left (motor mounting surface) and 291.6mm to the right (gearbox mounting surface). The load on the gearbox mounting side is 440N, and the load on the motor side is 580N. Considering a maximum 3G vertical acceleration, three holes are designed to bolt the

crossbar with the mounting plate with a diameter of 6 *mm*. The size of the rest of the mounting holes is defined by the hole size on the gearbox's mounting points.

3.1.2. FEA Modelling of the Crossbar and Analysis Results

To ensure the electric drive components are properly secured on the truck's ladder frame under various truck operation conditions. Load analysis on the crossbar was conducted using FEA modelling and simulations, as discussed below.

Boundary conditions of the crossbar are defined at the faces on both ends contacting with the frame as geometry A in Figure 10. The load at B represents the 439 N vertical gravity force. The torque load C represents the maximum 500 Nm output torque from the selected Cascadia iM-225 motor. The mesh element size is manually defined to be 0.015 mm for this simple geometry.

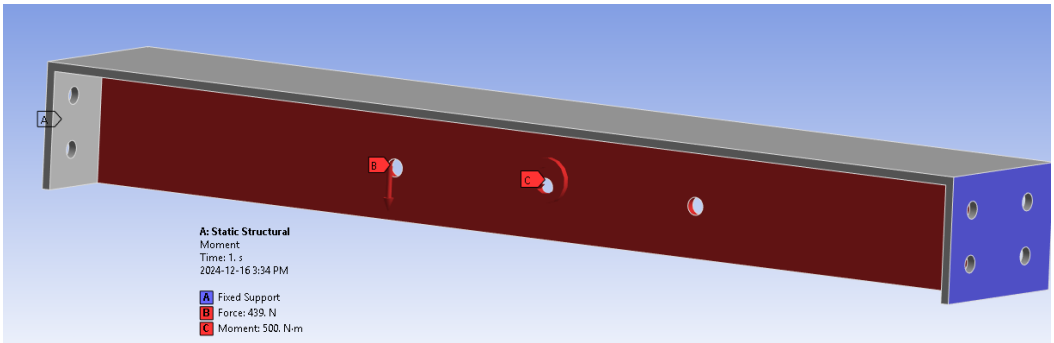

Figure 10: Crossbar FEA Modelling

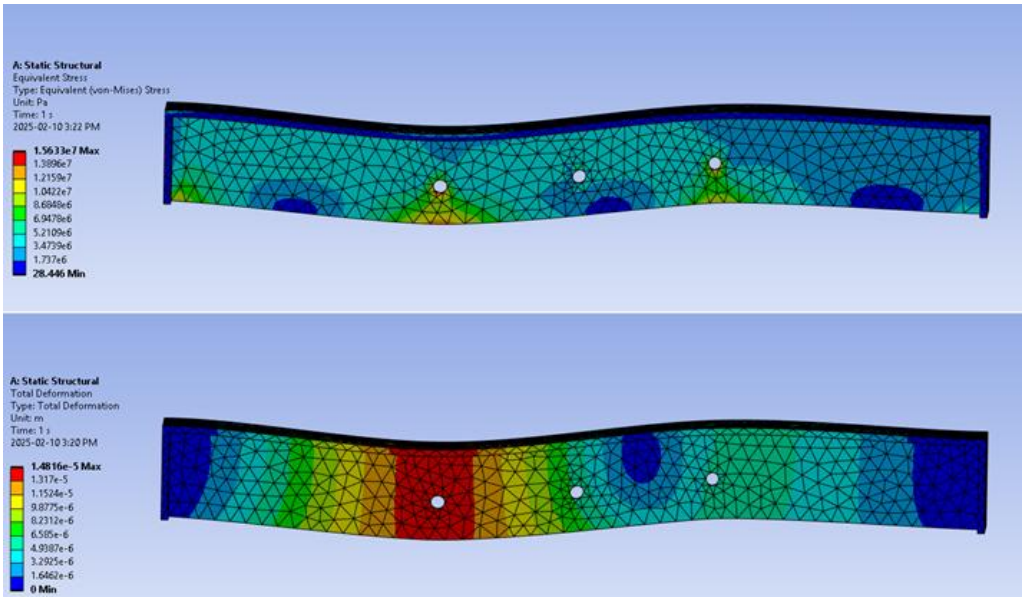

Figure 11: Total Deformation (top) and Equivalent Stress (bottom) of the crossbar

Figure 11 illustrates the crossbar's total deformation and equivalent stress under defined loading conditions. The maximum deformation, 0.01mm, occurs at the edge of the top surface. The

maximum stress, 7.52 MPa, appears at the corner of the middle face close to the fixed geometry on both sides, with a safety factor of over 15.

The fatigue load is defined as a fully reversed constant amplitude load. The object is subjected to alternating and compressive stress with a scaled factor of two while the mean stress is zero, as shown in Figure 12. The x-axle represents time (s), and y-axle is the scaling factor. Each fully reversed load cycle is assumed to last one second. The load is based on observing the UDDS driving cycle from 310 seconds to 780 seconds, which is relatively aggressive by driving the vehicle stop and go for 8 times. The average time for acceleration and deceleration is 46 seconds. The fatigue analysis defines the load in a more conservative scenario by reversing it in one second. The fatigue analysis results show that the component's life is infinite, with no damage demonstrated in Appendix C.

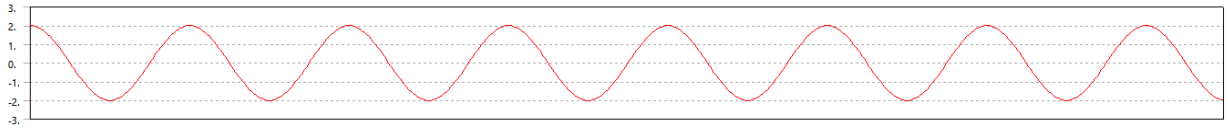

Figure 12: Fully Reversed Fatigue load for Gearbox Crossbar and Plate

3.1.3. FEA Modelling of the Gearbox Mounting Plate and Analysis Results

A gearbox mounting plate was designed and analyzed using a FEA model. The gearbox mounting plate has 10 mounting holes with a diameter of 0.85 mm, i.e., six on the plate and two on each flange. The fixed support in the FEA model is defined as the three holes bolted with a crossbar on the top, as shown on label A in Figure 13. A vertical weight load B, 439 N is applied to the mounting holes. The torque load C illustrated in Figure 13 is applied to the mounting holes.

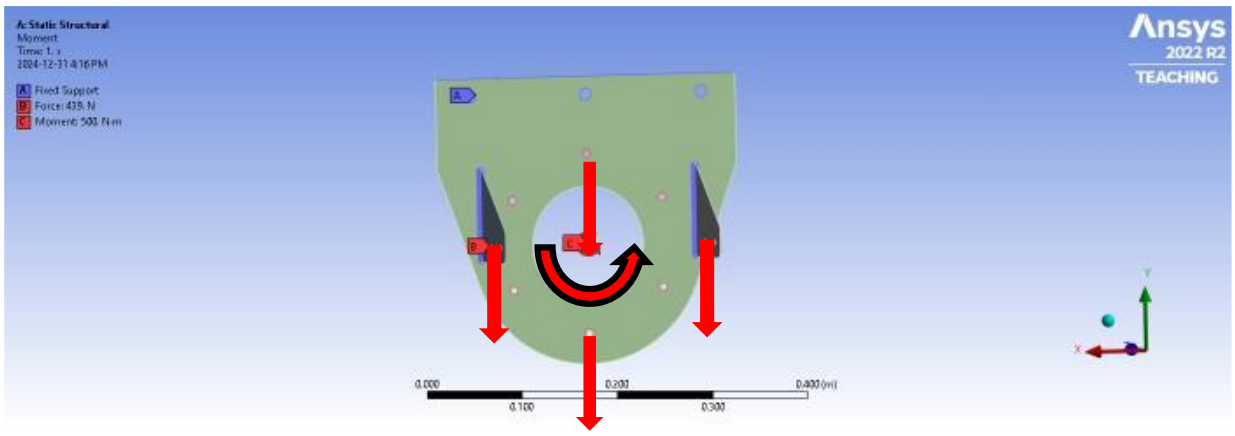

Figure 13: Gearbox Mounting Plate FEA Modelling

The mesh configuration defines the connection between the flange and the plate as continuous welding. To realize the welding mesh, batch control is required to be enabled. Batch control enables applying different mesh settings to individual parts. This model was turned into a shell model by generating mid-surfaces. The extended mid-surface function in shell model generation

must be turned off. The shell model must keep the gap between each plane because of the material thickness. Weld connection can only be applied to the shell model by selecting the edge and surface of the gap shown as the blue line at the bottom of each flange (Figure 13). The weldment material is the same as the component, meaning the welding wire requires more than 63,100 psi as the welded tensile strength. Therefore, a 0.035” diameter ER70S-6 weld wire was selected to have enough strength for the design.

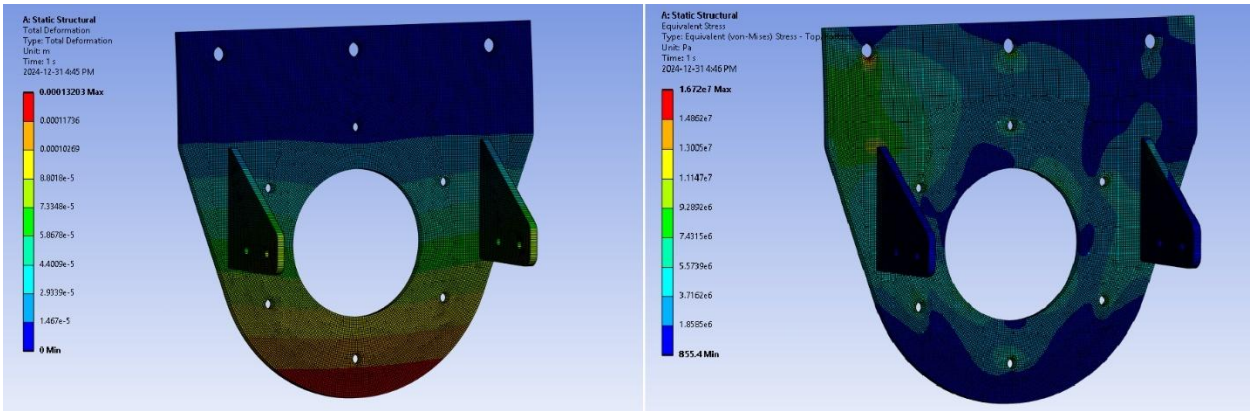

Figure 14: Total Deformation (Left) and Equivalent Stress (right) of plate

The safety factor for the static load simulation is required to be greater than 4. Due to time constraints, vibration and chatter effects are not considered in the simulation. To account for these unmodeled dynamic factors, the safety factor is increased from the conventional value of 2 for static loads to 4, ensuring a more conservative and reliable design.

From the results in Figure 14, the maximum deformation of 0.1 mm occurs at the lowest part of the plate. The maximum equivalent stress is 16.7 MPa, concentrated at the edge of the top left mounting hole. The stress safety factor is more than 15, as shown in Appendix C.

The fatigue load is the same as the crossbar simulation, as shown in Figure 12. The component’s life is infinite, and no damage occurs in the designed life. The minimum safety factor in fatigue analysis is 6.5, shown in Appendix C. It means that the load concentration will not cause any damage to the mounting holes.

3.2. Frame Redesign

The truck’s ladder frame is the key component as it supports the main powertrain components. The clearance requirements between the battery packs, the motor and gearbox installation points, and the driveshaft configuration influence the frame length. Figure 15 illustrates the 2D profile of the frame before extension. Two black circles represent the position of the wheels, with the short green vertical line indicating the position of the differential flange. The red lines are symmetrically tangent to the wheels, respectively. The red line on the right passes the bottom of the motor and gearbox. The angle between the red lines and the horizontal plane is called the breakover angle, which is mostly determined by the location of the motor and gearbox. Using this 2-D profile, the

layout of the powertrain can be decided, and the length of the extension can be calculated. Making the gearbox flange touch the differential flange without a driveshaft requires a 6.39-inch frame extension. To accommodate a 12-inch driveshaft with a 1-inch distance from the U-joint to the flange and maintain a 25-degree breakover angle, the drive shaft is raised to have a 12-degree angle with a horizontal plane. Under these constraints, the frame was extended by 20.53 inches, as shown in Figure 16. Based on this finalized layout, the frame requires an extension to reach a minimum length of 195 inches. Additionally, the existing cross members have been removed from the ladder frame to facilitate the integration of the new components. Under these revised conditions, the extended frame and battery packs must undergo structural analysis to evaluate their performance under the updated e-powertrain loads.

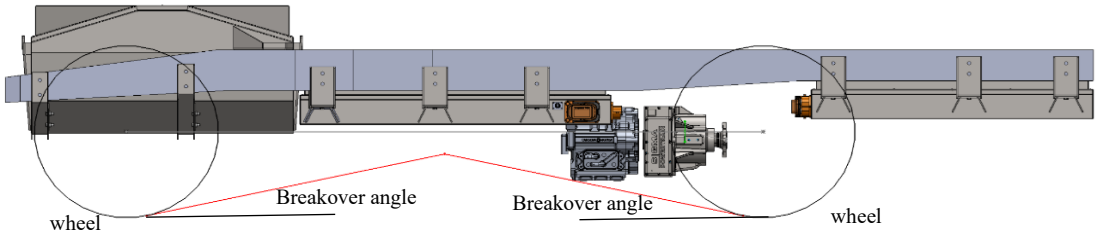

Figure 15: Initial Frame 2-D Profile

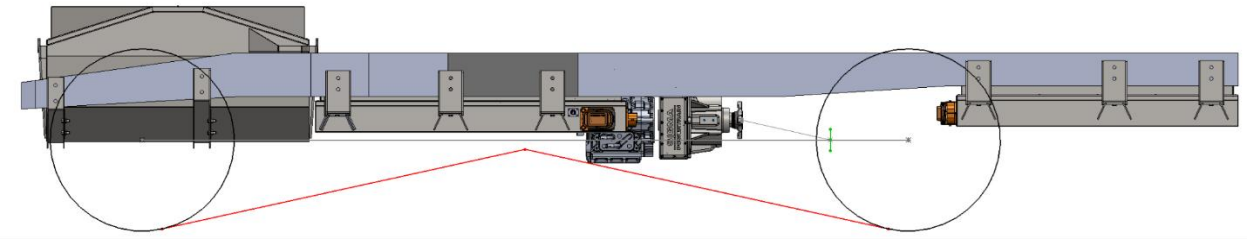

Figure 16: Extended Frame 2-D Profile

3.3. FEA Modeling and Analyses of the Frame

3.3.1. Simplification of Geometry

The CAD model of the ladder frame was created using the sheet metal modelling tools in SolidWorks to facilitate the generation of production drawings for the prototype vehicle. Due to the inherent gaps resulting from the sheet metal bending process, the initial model was not a closed rigid body. The CAD models for the battery enclosures were redesigned as rigid bodies, and non-structural components, such as the case lid and battery module holders, were excluded from the assembly to streamline the subsequent finite element analysis (FEA) study.

Including many intermittent seam welds would have resulted in over 100 overlapping connections during geometry preparation. To mitigate this issue, the weld connections between sheet metal components, including brackets and cross members, were removed and replaced with bonded connections in the FEA model. The weldment strength was assumed to be sufficiently rigid for the

frame strength analysis. To enhance mesh quality, the mounting holes on the brackets and frame were removed to reduce geometric complexity. Additionally, all fillets related to fabrication processes were removed in the redesigned models. However, critical edges that help mitigate load concentrations were retained to ensure the structural integrity of the simulation remains accurate.

This approach simplified the simulation setup while accurately representing the frame's structural behaviour.

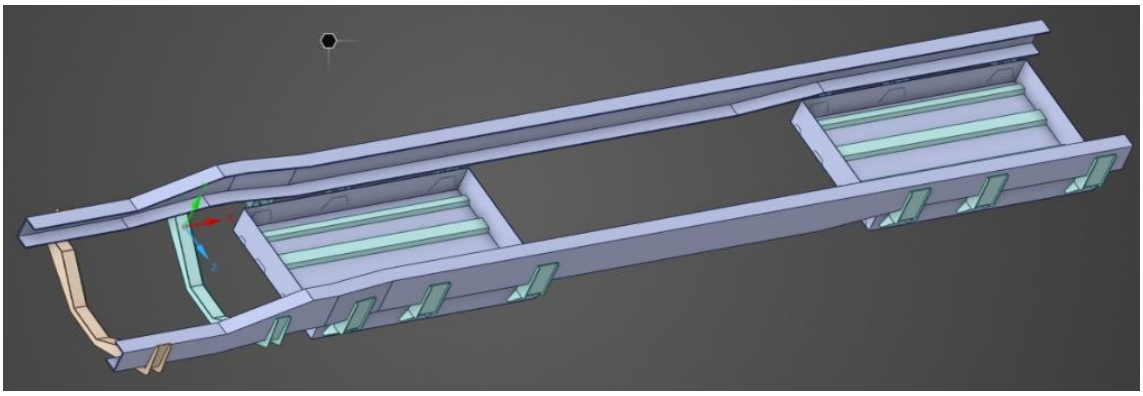

Figure 17 Simplified Geometry in ANSYS Discovery

3.3.2. Mesh

The frame geometry and battery cases were converted to shell models using the 'extended mid-surface' function during simulation preparation. This modification facilitated the automatic generation of connections between the brackets of the battery pack and the frame, ensuring successful mesh creation. Without employing the shell model approach, the complexity of the geometry would have led to mesh generation errors and poor mesh quality.

The mid-surface of the frame was refined to level three, significantly enhancing the average element metrics from 0.31 to 0.56, as detailed in Appendix C. Figure 20 illustrates the overall mesh result of the assembly after refinement. Figure 18 highlights the improved mesh quality of the frame. In contrast, the corresponding Figure 19 demonstrates that the element metrics of the frame (shown in purple) achieve a higher than 0.5 value, with most elements having values close to 1, showing a high-quality mesh.

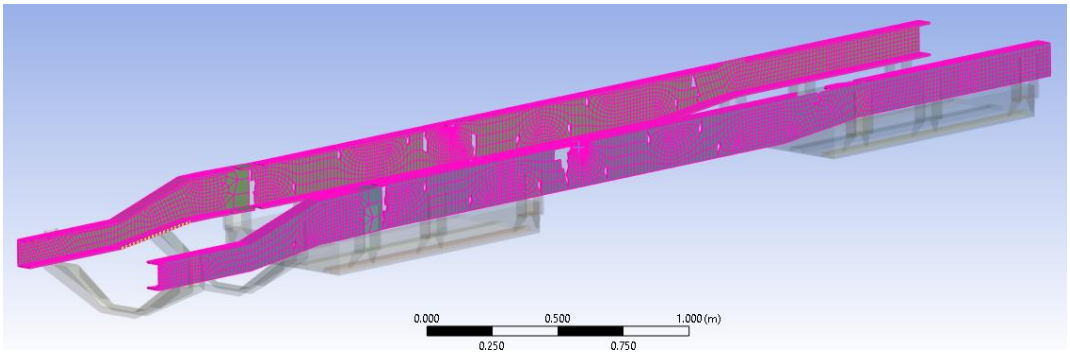

Figure 18: Mesh of Frame

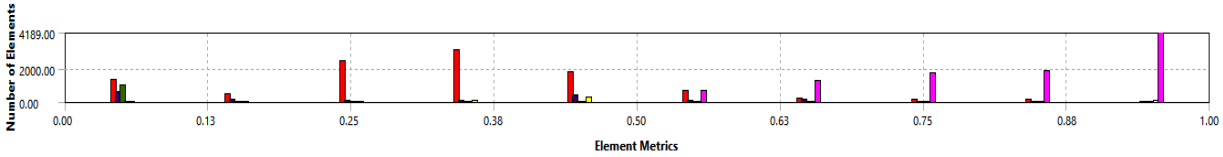

Figure 19: Element Metrics for Frame

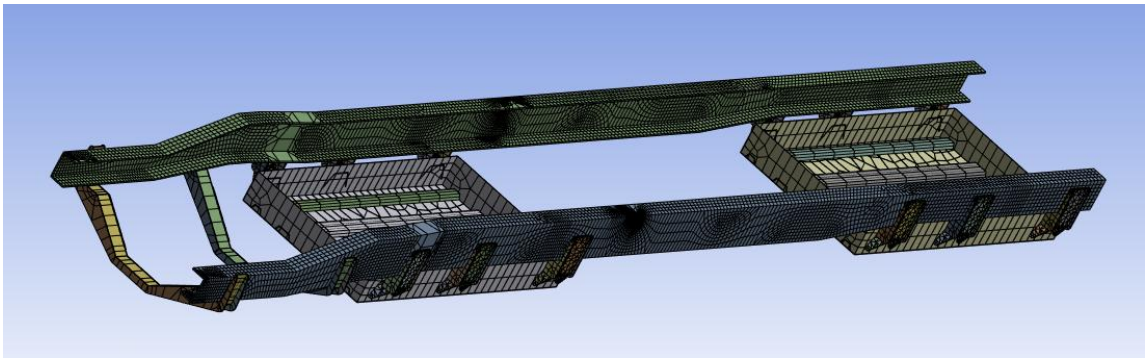

Figure 20: Mesh of the Extended Frame and Cross Members

3.3.3. Boundary and Loading Conditions

For the front battery pack load, the battery case, containing four battery modules, is supported by the structural cross beam. The total weight of the front pack, 398.32 kg, is evenly distributed across the contact surface, resulting in a vertical stress of 55,706 Pa.

The mid-pack and rear-pack house three battery modules, each weighing 300.22 kg per pack. These modules are bolted onto C-channel beams, distributing the weight evenly across the beams. This design results in a vertical stress of 2,056 Pa, as illustrated in Figure 21.

Figure 22 shows the remaining external loads applied to the system, including the motor and gearbox, the Cabin, and the truck bed at the rear of the frame. The motor and gearbox load comprises two primary components, load C and A, as shown in Figure 22: the combined weight of the motor and gearbox assembly and the torque corresponding to the motor's maximum output torque. The load is applied at the center of gravity of the entire assembly.

Since no specific physical point in the geometry represents this load, the ‘remote point’ function defined the torque along the longitudinal axis. The remote point behaves as a rigid body and is applied to the frame’s motor and gearbox mounting surface, ensuring the simulation captures the load’s effect.

The truck bed load is modelled as sitting on the top surface of the frame, spanning a length of 2590.8 mm (102 inches). Load B represents a worst-case scenario, corresponding to the truck’s maximum payload capacity of 1066.6 kg, as calculated in the previous section. This payload is uniformly distributed over the rear frame surface, resulting in a vertical stress of 35,949 Pa.

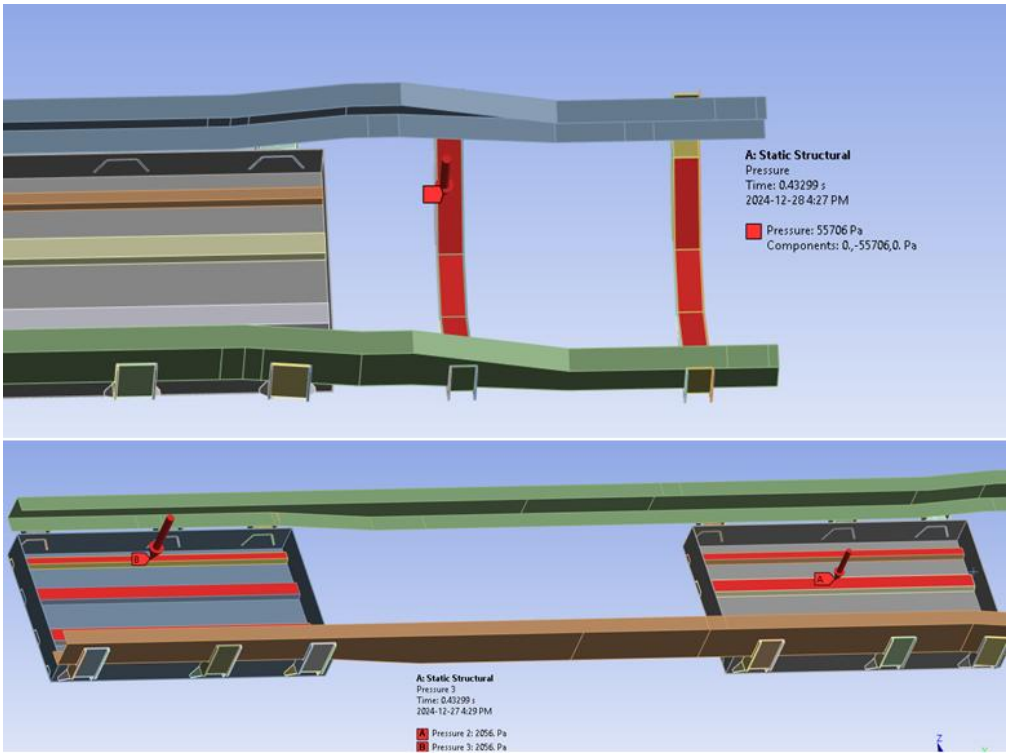

(A): Middle Pack Load 2056 Pa (B): Rear Pack Load 2056Pa

Figure 21: Front Pack and Middle Pack Loading Conditions

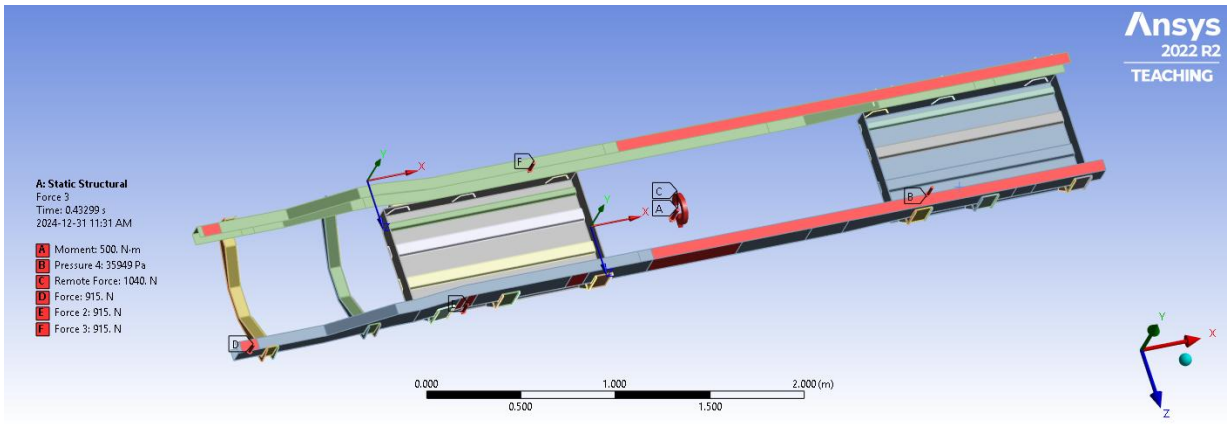

Figure 22: External Loads Excluding Battery Packs

The cabin load is represented by three vertical forces, load D, E and F, shown in Figure 22. Each force is 915 N, symmetrically applied to the top and side surfaces of the frame at locations corresponding to the front, center, and rear 'Cab Mounts,' detailed in the weight distribution section.

The fixed geometry at the mounting brackets of the original Toyota Dyna frame defines the boundary conditions. Since the Dyna suspension system will be retained in the prototype vehicle, the relative positions of the suspension mounting brackets will be preserved. As illustrated in Figure 23, fixed geometry A represents the front suspension mounted beneath the frame. Fixed geometry B represents the bracket mounting point on the outer side of the frame for the rear leaf springs. This setup accurately simulates the frame's structural behaviour under the applied loads.

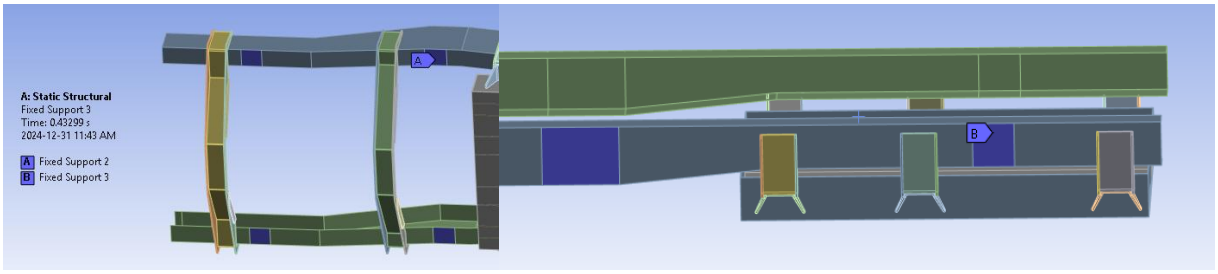

Figure 23: Fixed Suspension Mounting Geometry

3.3.4. Material properties

As shown in Figure 24, the frame material is specified as a hot-rolled steel plate with a tensile strength of 440 MPa and a yield strength of 304 MPa. Since no additional material information is provided in the manual, the material used in the simulation is modelled as 'Carbon Steel, 1020, as rolled,' which has a tensile strength of 444 MPa and a yield strength of 328 MPa.

Compared to the original material, Carbon Steel 1020 exhibits improved stiffness properties as rolled. To compensate for any potential deviations between the simulated and actual frame

materials, a relatively high design factor of safety is applied to ensure the structural integrity and reliability of the redesigned frame under operational conditions.

FRAME MATERIALS

TOYOTA DYNA truck series use the following frame materials;

MATERIAL			APPLICABLE MODELS
Type of metal	Tensile strength	Yield strength	
Hot rolled steel plate	440N/mm^2 { 45kgf/mm^2}	304N/mm^2 { 31kgf/mm^2}	Standard cab series (XZU300 series)
Hot rolled steel plate	540N/mm^2 { 55kgf/mm^2}	392N/mm^2 { 40kgf/mm^2}	Wide cab series (XZU400 series)

Figure 24: Frame Materials of Dyna Truck in Body Builder Guidebook [15]

3.3.5. FEA Results

The deformation of the assembled frame is depicted in Figure 25. The maximum deformation, measuring 0.2 mm, occurs on the bottom surface of the middle battery pack. Additionally, the frame exhibits a maximum deformation of 0.10 mm at the cabin rear mount, as shown in Figure 26.

The overall assembly results indicate a maximum Von Mises stress of 109 MPa, located at the front pack cross beam, corresponding to a factor of safety 3.0. When isolating the ladder frame, the maximum Von Mises stress is reduced to 22.23 MPa, occurring near the suspension mounting surface on the side frame shown in Figure 27. The minimum safety factor for concentrated loads in the system is calculated to be 14.7, ensuring high structural reliability.

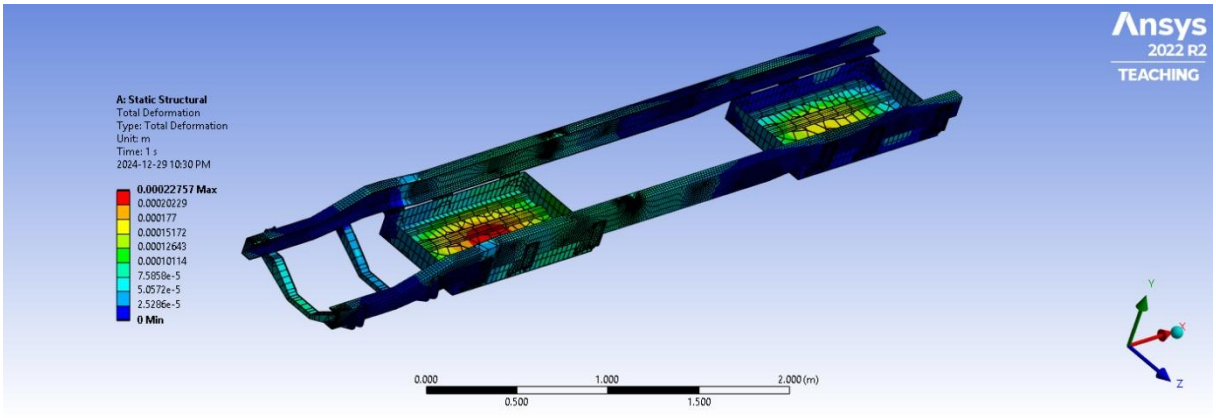

Figure 25: Total Deformation of the Assembly

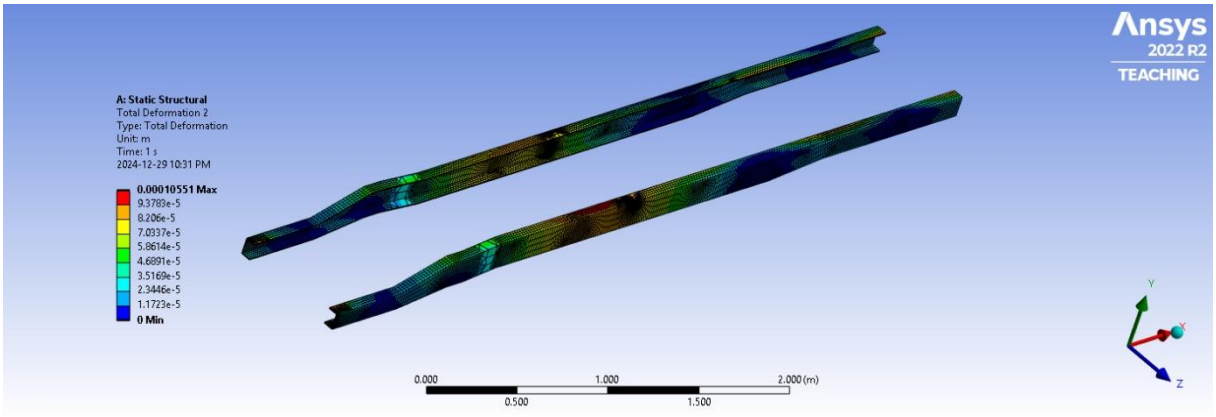

Figure 26: Deformation Result of Frame

In the fatigue analysis, the stress component selected is the Von Mises stress derived from the static simulation. The loading condition is defined as a fully reversed load, the same as the previous fatigue analysis, as illustrated in Figure 28. The Goodman mean stress correction theory is applied to account for the effects of mean stress under this constant amplitude loading condition. The safety factor of fatigue analysis of the ladder frame is 8.7, as shown in Figure 49.

Based on these parameters, the minimum calculated fatigue life of the frame is 10^8 cycles, corresponding to 8 hours of operation per day for 9 years, ensuring the frame's durability under the specified loading conditions. This design life is the required working lifetime for the prototype vehicle from CanEV.

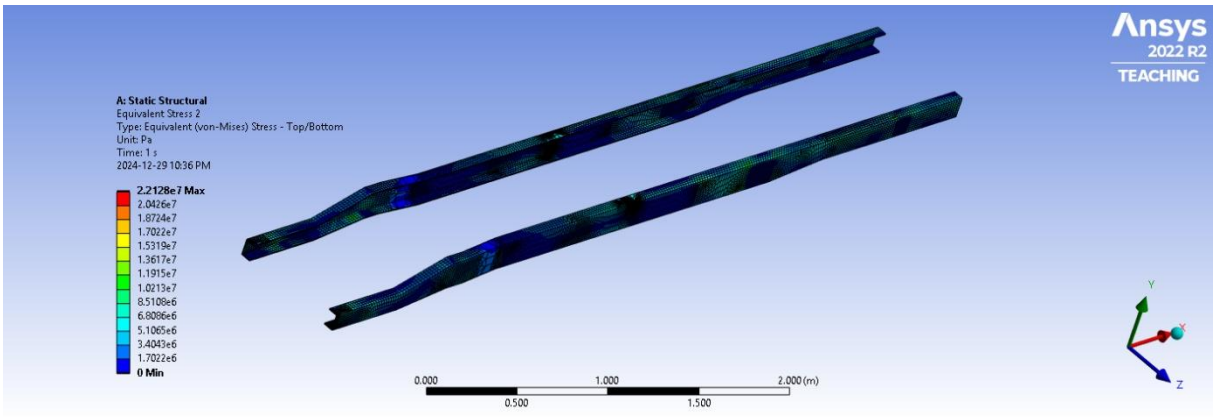

Figure 27: Equivalent (Von-Mises) Stress Result of Frame

As discussed earlier, the fatigue load is a fully reversed constant amplitude load. The x-axle represents time (s), and y-axle is the scaling factor. Each fully reversed load cycle is assumed to last one second. The load is based on observing the UDDS driving cycle from 310 seconds to 780 seconds, which is relatively aggressive by driving the vehicle stop and go for 8 times. The average time for acceleration and deceleration is 46 seconds. The fatigue analysis defines the load in a

more conservative scenario by reversing it in one second. The fatigue analysis results show that the component's life is infinite, with no damage demonstrated in Appendix C.

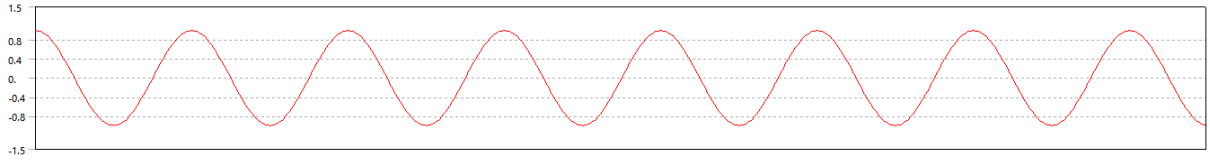

Figure 28: Fatigue Analysis Input Load

The results indicate that the extended frame provides sufficient stiffness to accommodate the electric powertrain and a fully loaded truck bed at the rear. Compared to the original frame structure, the cross members have been removed, and the frame has been extended longitudinally by 20.53 inches to integrate the 10 battery modules, motor, gearbox, and drive shaft. Also, the Dyna 350 series wheelbase is 31 inches longer than the prototype truck. Therefore, the extension solution uses an existing Dyna 350 truck frame and will not change the truck's roadworthiness. Summary

This chapter focuses on the design and analysis of the crossbar, the gearbox mounting plate, and the frame. Both static structural analyses and fatigue analyses have been conducted on all components. The results show that the designs have high safety factors and are thus satisfactory. Existing sheet metal materials are chosen to ensure low material and fabrication costs.

The next chapter will introduce topology optimization and hyperparameter optimization basics, paving the way for Chapter 5, in which these techniques will be applied to the third customized-component design, the motor bracket design.

4. Hyperparameter Optimization for Topology Optimization Algorithm

4.1. Introduction

One of the major challenges of EV design and retrofitting is the significant increase in vehicle weight due to the addition of BESS and electric drive. Application of the Solid Isotropic Material with Penalization (SIMP) topology optimization algorithm, coupled with hyperparameter optimization (HPO), for possible weight reduction for the e-MDT is tested using the motor bracket design as an example for component weight reduction.

Minimizing the electric powertrain's weight increases the design space and load-carrying capability for cargo within the total gross vehicle weight constraints. This work applies topology optimization to the bracket design for weight reduction. Topology optimization, specifically the Solid Isotropic Material with Penalization (SIMP) algorithm, is a powerful tool for determining optimal material distribution within a design space. However, its performance is heavily influenced by key hyperparameters such as volume fraction, penalization factor, filter radius, and move step size. The design problem was formulated as follows.

The bracket material is 1020 Carbon Steel (as-rolled) sheet metal, with a tensile yield stress of 328.1 MPa and a 7.89 g/cm³ density. The sheet metal is designed with a thickness of 12.7 mm (0.5 inches). The bracket is mounted to the bottom of the ladder frame at one end and bolted to the Cascadia IM-225 motor at the other. Figure 29 illustrates the bracket's spatial design area and initial design dimensions.

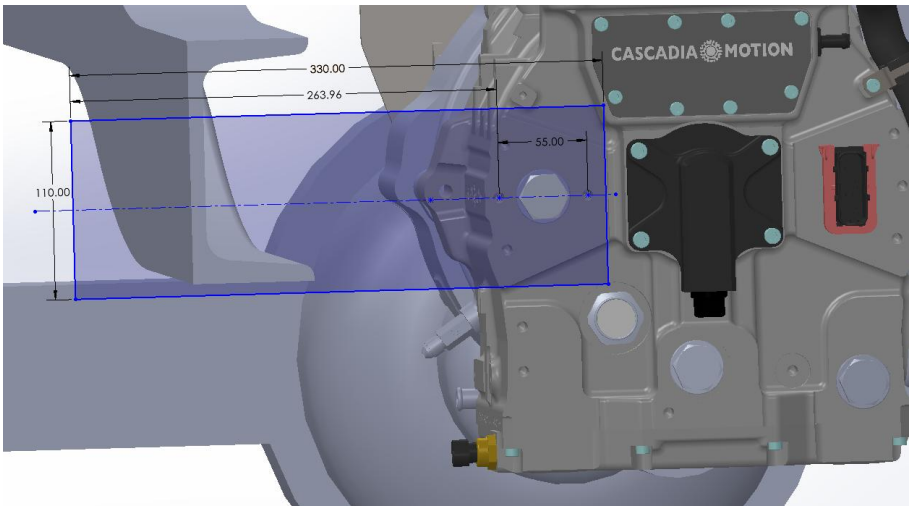

Figure 29 Bracket Design Space and Dimensions (blue sketch area)

4.2. Initial Design and FEA modelling

The initial design of the bracket is a rectangular plate with mounting holes. This configuration represents the simplest geometry that can be fabricated from sheet metal, allowing the problem to be modelled as a cantilever beam subjected to a torque load. Figure 30 illustrates the sketch and CAD model of the plate. To enable topology optimization in subsequent design stages, the dimensions were simplified to an overall length of 330 mm and a width of 110 mm.

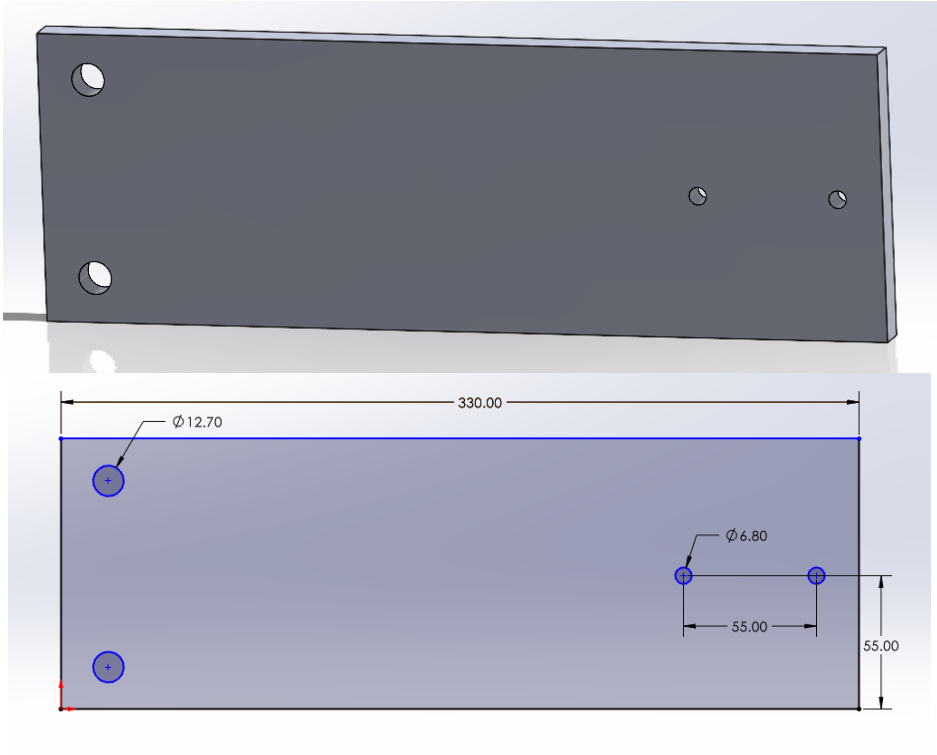

Figure 30 Initial Bracket Design

The Cascadia IM-225 motor and Sigma Powertrain gearbox weigh 102 kg, generating a peak torque of 500 Nm, serving as the bracket's primary loading condition. The mounting holes on the bracket are fixed, with a spacing of 55 mm, as shown in Figure 30. The deadweight load from the gearbox and motor assembly on each bracket side is calculated to be 290 N. However, the motor's output torque is converted into a force couple of 4545 N at the mounting holes. The detailed calculation process is provided in Appendix C. Given the larger than one order of magnitude difference between these forces, the smaller deadweight load is disregarded for the design.

Two mounting holes on the left side of the bracket are defined as fixed boundary conditions. The applied force loads, represented by red vectors, are shown in the FEA model in Figure 3. ANSYS Workbench is used for FEA modelling and analysis. The input is modelled as a fully reversed load for fatigue analysis, amplified by a scale factor of two, as illustrated in Figure 32. The x-axle is time, and the y-axle is the scale factor to amplify the static loads.

4.3. FEA results

The FEA of the initial design reveals a maximum Von-Mises stress of 60.8 MPa, corresponding to a static safety factor of 5.399. Fatigue analysis indicates that the structure sustains zero damage under infinite loading cycles, with a fatigue safety factor 2.78. These results suggest that the structure is excessively stiff and presents opportunities for weight reduction without compromising its performance.

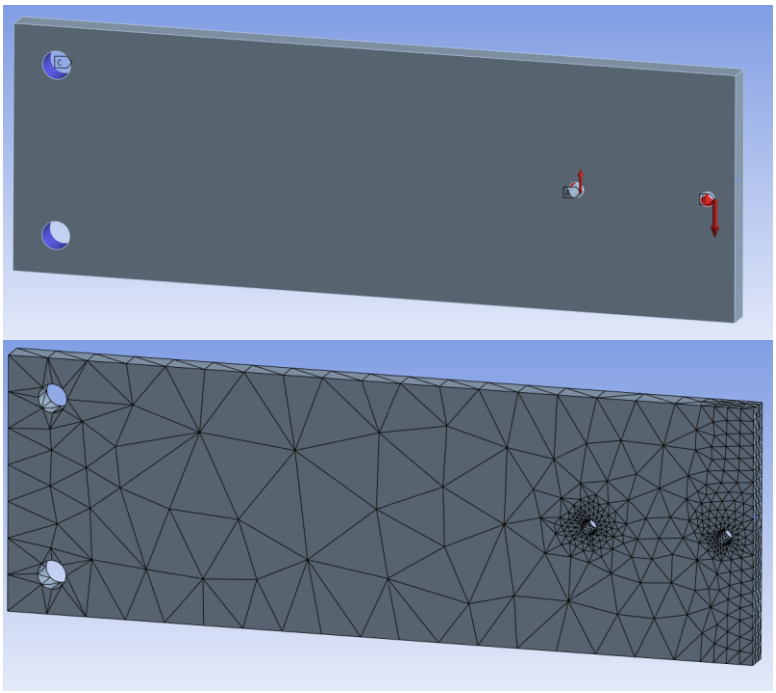

Figure 31 FEA Model and Mesh

Again, a similar fatigue load is applied. The x-axle represents time (s), and y-axle is the scaling factor. Each fully reversed load cycle is assumed to last one second.

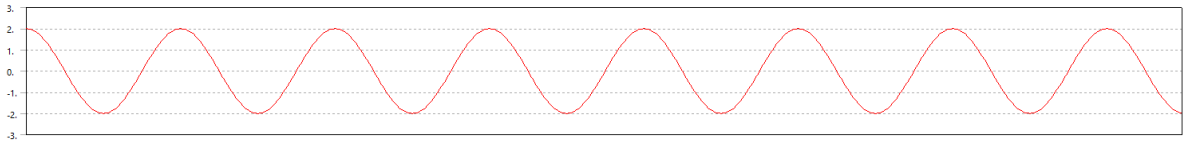

Figure 32 Cyclical Loading for Fatigue Analysis

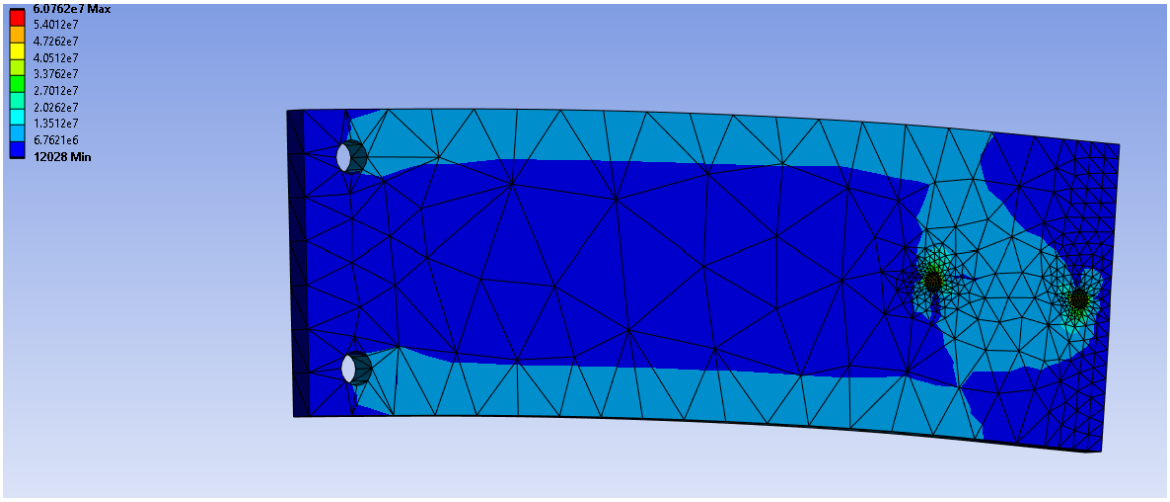

a. Von Mises Stress Plot

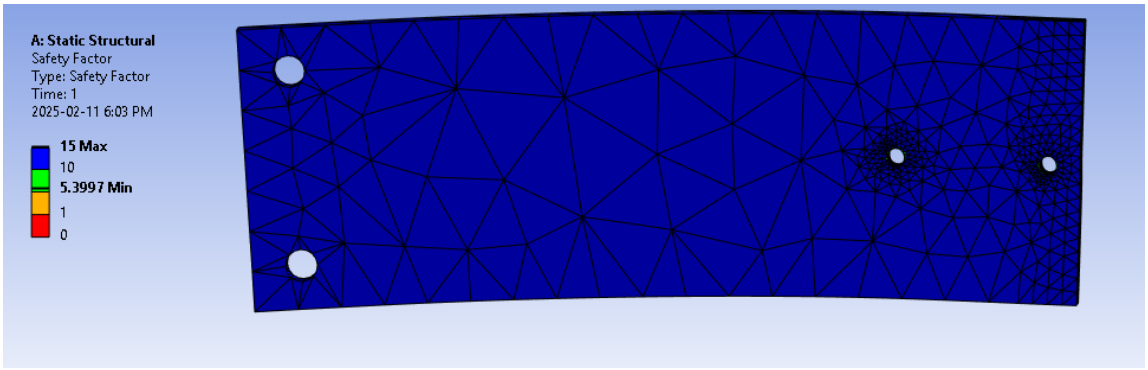

b. Safety Factor Plot under Fatigue Analysis

Figure 33 FEA Results for the Initial Design, a. Von Mises Stress Plot, and b. Safety Factor Plot under Fatigue Analysis

4.4. Overview of Topology Optimization

Topology optimization (TO) is a structural design technique determining the optimal material distribution within a defined design space. The objective is to maximize structural performance while adhering to constraints such as weight, loading conditions, and fixed geometry[16]. Unlike traditional design methods, which rely on predefined shapes, topology optimization begins with a broad design space and iteratively removes material to achieve an optimal configuration. This topology optimization approach is widely applied in industries such as automotive[17], aerospace[18], bioengineering[19], and civil engineering [20].

The design domain is discretized into elements and nodes within a FEA model in topology optimization. Numerical equations and relationships between displacements and loads govern these discrete elements and nodes. The optimization objective, compliance, is defined as the sum of the compliance of individual components. Numerically, compliance is equal to twice the elastic

energy of the structure. The algorithm does not account for the structure's material properties, and Young's modulus is set to unity. As a result, compliance is best treated as a no-unit variable in this method.

The (Solid Isotropic Material with Penalization) approach assumes constant material properties within each element [21], [22]. The density of the elements, which serves as the design variable, ranges between 0 (void) and 1 (solid). A penalization scheme drives intermediate density values towards 0 or 1, creating a clear and more manufacturable design.

4.5. Algorithm Selection and Code Analysis

The integrated Topology Optimization code adopted in this project is the 99-line top' MATLAB code[23]. This 2-D topology optimization code allows for the definition of fixed geometry boundary conditions and multiple nodal force loads. The problem is formulated using the following equations:

$$Minimize \quad c(x) = U^T K U = \sum_{e=1}^{N} (x_e)^p {u_e}^T k_0 u_e \tag{6}$$

$$\text{Subject to:} \quad \begin{aligned} \frac{V(x)}{V_0} &= v_{fraction} \\ KU &= F \\ 0 < x_{min} &\leq x \leq 1 \end{aligned} \tag{7}$$

where U and F are the global displacement and force vectors. K is the global stiffness matrix. u_e and k_e are the element displacement vector and stiffness matrix, respectively. x is the vector of design variables, x_{min} is a vector of minimum relative densities from zero to one. N (= *nelx* **x** *nley*) is the number of elements that discretize the design domain. p is the penalization power factor; the default value is 3. $V(x)$ and V_0 are the material and design domain volumes, respectively. In the code, $v_{fraction}$ is the volume fraction as defined in constraints [23].

The design variable is updated by a standard Optimality Criteria (OC) method, which is heuristically formulated as

$$x_e^{new} = \begin{cases} \max(x_{min}, x_e - m) & if\ x_e B_e^{\eta} \leq \max(x_{min}, x_e - m) \\ x_e B_e^{\eta} & if \max(x_{min}, x_e - m) < x_e B_e^{\eta} < \min(1, x_e + m) \\ \min(1, x_e + m) & if\ \min(1, x_e + m) \leq x_e B_e^{\eta} \end{cases} \tag{8}$$

$$B_e = \frac{-\frac{\partial c}{\partial x_e}}{\lambda \frac{\partial V}{\partial x_e}} \tag{9}$$

where m (move) is a positive move-limit, η (= 1/2) is a numerical damping coefficient. λ is a Lagrangian multiplier found by a bi-section algorithm. The OC method updates distributed element density while satisfying the volume fraction constraints and improving the objective function.

A filter technique is applied to the algorithm by modifying the element sensitivities as follows:

$$\frac{\widehat{\partial c}}{\partial x_e} = \frac{1}{x_e \sum_{f=1}^{N} \widehat{H_f}} \sum_{f=1}^{N} \widehat{H_f}\, x_f \frac{\partial c}{\partial x_e} \tag{10}$$

$$\frac{\partial c}{\partial x_e} = \frac{1}{p} (x_e)^{(p-1)} {u_e}^T k_0 u_e \tag{11}$$

where the convolution operator $\widehat{H_f}$ is written as:

$$\begin{gathered} \widehat{H_f} = r_{min} - dis(e,f) \\ \{f \in N \mid dis(e,f) \leq r_{min}\} \end{gathered} \tag{12}$$

where $\frac{\partial c}{\partial x_e}$ is the original sensitivity of the objective function. $dis(e,f)$ is defined as the distance between elements e and f. r_{min} is a heuristic parameter as the minimum filter radius. The operator $\widehat{H_f}$ is zero if element f is outside of the filter area.

The filter ensures the gradual change in element density, which reduces the possibility of checkboard, alternating high and low densities in adjacent elements caused by numerical instability.

This SIMP algorithm involves a couple of parameters that a user has to set. To understand the influences of these parameters and achieve the best possible combination of these parameters, I looked at hyperparameter optimization (HPO).

4.6. Introduction of Hyperparameter Optimization

Hyperparameter Optimization (HPO) is a systematic process used to determine the best parameter combinations for a machine learning or optimization algorithm to maximize performance on a specific task [24]. Common HPO methods include Grid Search[25], Random Search[26], and Bayesian Optimization [27]. Application of heuristic optimization methods, such as Genetic Algorithm (GA), Particle Swarm Optimization (PSO), Simulated Annealing Method (ASM), and Machine Learning (ML), often involves tuning hyperparameters.

Grid Search systematically evaluates all combinations of hyperparameters within defined ranges and is particularly suited for small-scale problems. On the other hand, Random Search explores the hyperparameter space by sampling randomly. At the same time, Bayesian Optimization uses a probabilistic surrogate model to predict the relationship between hyperparameters and model performance, making it well-suited for functions with high evaluation costs.

These HPO methods are primarily tailored for machine learning applications[28]. In this project, to gain insight into the hyperparameters and filter out the unimportant parameters, the Design of Experiments (DOE) approach was used to screen four hyperparameters. A response surface model was then employed to represent the relationship between the parameters (factors) and the response (final compliance). Subsequently, a gradient-based optimization method was applied to identify the optimal combination of parameters to minimize compliance. This approach offers intuitive and visualizable results.

From the implementation of the 99-line MATLAB code, there are four heuristic parameters defined:

- $v_{fraction}$: volume fraction between the optimal and original design.
- p: penalization power factor in SIMP.
- r_{min}: filter radius to average the sensitivities over the neighbourhood.
- $move$: move step size to update the element density.

These four parameters are chosen as hyperparameters of the TO algorithm for the ensuing study. Besides, these parameters are no-unit variables. Specifically, the r_{min} is calculated by the distance of the element index in the design space, so this algorithm has no unit for this filter radius.

4.7. Hyperparameters Analysis Using ANOVA

4.7.1. Principles and Objectives of DOE

Design of Experiments (DOE) is a systematic approach to planning, conducting, analyzing, and interpreting controlled tests to evaluate the factors influencing a response.

In the context of Hyperparameter Optimization, the DOE method serves as a preliminary step[29]. It is used to screen multiple variables, reducing the number of factors (parameters) to a smaller, more manageable group by identifying the key parameters and the most effective combinations.

4.7.2. DOE Results and Hyperparameters Selection

Four hyperparameters are considered as four factors in DOE. Compliance is the output response.

$$\begin{gathered} 0.1 \leq move \leq 0.3 \\ 2 \leq p \leq 4 \\ 1 \leq r_{min} \leq 3 \\ 0.5 \leq v_{fraction} \leq 0.7 \end{gathered} \tag{13}$$

The design space of parameters is shown above. Table 5 displays the data set generated using a full factorial design, which tests all possible combinations at two levels for each factor. The full factorial design approach was chosen to preserve a relatively large design space by setting the level values at the boundaries of the design domain. This method ensures that the combinations of

experiments explore the most extreme points of the design space, allowing for comprehensive coverage and simultaneous acquisition of insights through testing.

Four combinations of factors, as shown as "NC" in Table 5 did not converge. The primary reason for this instability is the simultaneous use of a large penalization power factor p and a large r_{min}. This combination results in numerical instability, as an excessively large filter area leads to overshooting when the penalization power is also high.

Table 5 DOE Data Set

move	*P*	r_{min}	$v_{fraction}$	compliance
0.1	2	1	0.7	204.027
0.3	2	1	0.7	204.0546
0.1	2	2	0.7	216.8498
0.3	2	2	0.7	216.8669
0.1	2	1	0.5	265.1601
0.3	2	1	0.5	267.1283
0.1	2	2	0.5	315.073
0.3	2	2	0.5	315.2507
0.1	4	1	0.7	213.0574
0.3	4	1	0.7	217.9187
0.1	4	2	0.7	NC
0.3	4	2	0.7	NC
0.1	4	1	0.5	296.2223
0.3	4	1	0.5	312.9907
0.1	4	2	0.5	NC
0.3	4	2	0.5	NC

The most critical parameters and their interactions influencing topology optimization were identified using the 'ANOVAN' function in the MATLAB toolbox. As shown in Figure 34, hyperparameters $v_{fraction}$, $r_{min,}$ and p exhibit relatively low p-values, indicating that these three parameters and their interactions have the most significant impact on the final compliance. Consequently, the hyperparameter *move* was excluded from further analysis.

Analysis of Variance

Source	Sum Sq.	d.f.	Mean Sq.	F	Prob>F
move	47.3	1	47.3	0.41	0.5443
p	1245.5	1	1245.5	10.69	0.0137
rmin	1911.8	1	1911.8	16.41	0.0049
volfrac	20754.3	1	20754.3	178.2	0
Error	815.3	7	116.5		
Total	23769.1	11			

Figure 34: ANOVA Results for Four Hyperparameters

4.8. Optimization and Response Surface Modelling of Hyperparameters

The Hyperparameter Optimization problem can be modelled as follows:

$$Minimize\ f\left(p, r_{min}, v_{fraction}\right) = c \tag{14}$$

$$2 \leq p \leq 4$$
$$1 \leq r_{min} \leq 3$$
$$0.5 \leq v_{fraction} \leq 0.7$$

The objective function is the 3-level response surface model, which predicts the relationship between hyperparameters and final compliance in topology optimization.

The methodology for the response surface modelling employed is the Box-Behnken Design (BBD). This approach utilizes center points without necessitating experiments at extreme levels for all factors. Table 6 presents the three-level DOE data set generated using the Box-Behnken Design. Compared to a full factorial design, this method requires fewer experiments, making it more efficient.

Another advantage of the Box-Behnken Design (BBD) is its ability to avoid corner points in the design space, where data convergence issues were observed in the previous Analysis of Variance. This feature enhances the accuracy of the response surface model by focusing on regions of the design space that are more stable and reliable.

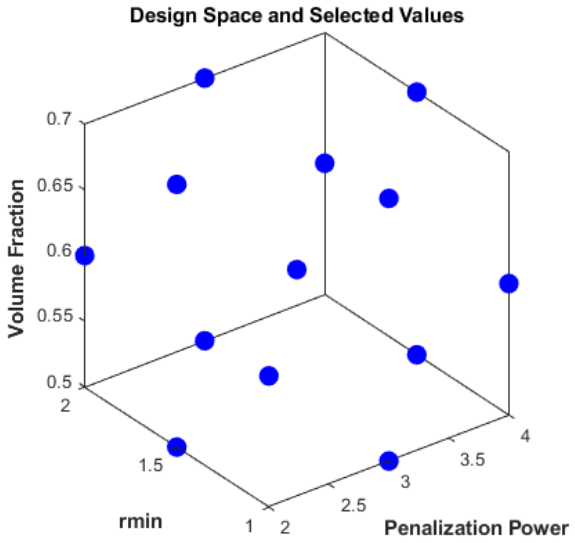

Figure 35 Design Space and Selected Values in BBD

Table 6 Box-Behnken Design Data Set

p	r_{min}	$v_{fraction}$	compliance

2	1	0.6	223.2687
2	2	0.6	236.9124
4	1	0.6	257.3035
4	2	0.6	240.6797
2	1.5	0.5	270.5963
2	1.5	0.7	209.9943
4	1.5	0.5	277.9859
4	1.5	0.7	212.2445
3	1	0.5	281.4267
3	1	0.7	208.9432
3	2	0.5	280.0312
3	2	0.7	212.7028
3	1.5	0.6	236.14
3	1.5	0.6	236.14
3	1.5	0.6	236.14

4.9. Solution of Hyperparameter Optimization for Topology Optimization Problem

The code for building the response surface model, sensitivity analysis, and optimization can be found in Appendix D.

Figure 36 presents the predicted response plot for the variables p, r_{min}, and $v_{fraction}$ shown from left to right as a full quadratic model. Among these, $v_{fraction}$, has the most significant influence on the response, while r_{min} has the least. Surface plots illustrating the interactions between these variables are provided in Appendix E.

The response surface model achieves an R-squared value of 0.987053, indicating high predictive accuracy. The parameters yielding the minimum compliance in the topology optimization code were identified using the 'fmincon' function from the Optimization Toolbox in MATLAB.

The solution of Hyperparameter Optimization is $[p, r_{min}, v_{fraction}] = [2, 1, 0.7]$ which returns a compliance value of 199.25. Then, the difference between the actual and predicted compliance is 1.13%.

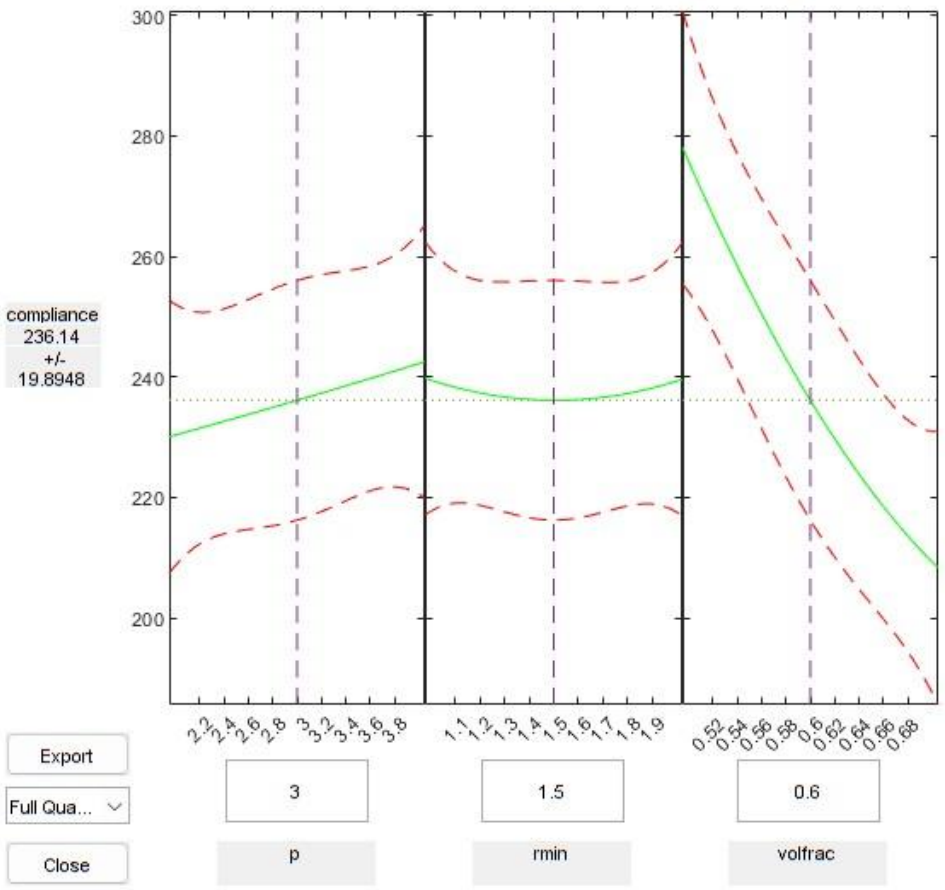

Figure 36 Predict Plot of Full Quadratic Model

```
The R-square value is 0.987053


Optimal Values:
  p:        2 mm
  rmin:       1 mm
  Volfrac:     0.7 mm
```

```
>> fval

fval =

       199.25
```

```
 The actual optimal function value is  201.54 . The difference is 1.13715 percent.
```

Figure 37 Hyperparameter Optimization Solution

Table 7 Optimal Designs Comparison

Element size 66x22	Rectangular	Default TO	HPO-TO
p	3	3	2
r_{min}	1.5	1.5	1
$v_{fraction}$	1	0.7	0.7
compliance	181.4778	219.5302	201.54
Optimized structure			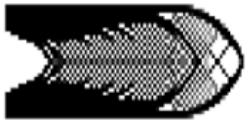

Table 7 summarizes the results from the initial design, default topology optimization, and the TO with optimal hyperparameters (HPO-TO). Compared to the initial design, TO and HPO-TO achieved a 30% weight reduction with higher compliance. Compared with the default TO, HPO-TO led to an 8% improvement in compliance with the same loading conditions and weight. However, a limitation of the optimized parameters is that the resulting plate structure is challenging to parameterize and shows a checkboard.

4.10. Summary

Chapter Four introduces the application of the Solid Isotropic Material with Penalization (SIMP) topology optimization algorithm, coupled with hyperparameter optimization (HPO), for possible weight reduction for the electric medium-duty truck (e-MDT) components. The focus is on optimizing material distribution for structural efficiency. Four key hyperparameters—volume fraction, penalization factor, filter radius, and move step size are critical to the optimization. Using a systematic Design of Experiments (DOE) approach, the study evaluates the influence of these hyperparameters on optimization outcomes. Box-Behnken Design is employed in a reduced design space, in which a response surface model is developed to map the relationships between hyperparameters and the structure compliance, the optimization objective.

The results validate the significance of hyperparameter tuning, demonstrating improvements in compliance and structural performance over default optimization settings. The insights gained from this chapter form the foundation for Chapter Five, where the optimized parameters are applied to the motor bracket design.

5. Application of Topology Optimization on Bracket Design

The topology optimization algorithm with optimized hyperparameters is applied to the design of the motor bracket for the e-MDT, transitioning from theoretical exploration to practical implementation. The objective is to minimize the bracket's weight while maintaining its structural integrity under static and dynamic loads, ensuring it meets the vehicle's performance and reliability requirements. Building on the optimization techniques developed in Chapter Four, the topology results are parameterized into CAD models, and finite element analysis (FEA) is conducted to validate its performance. By comparing the initial design, optimized design with default settings, and optimized design with HPO, this chapter demonstrates how advanced optimization techniques can achieve a lightweight and structurally robust design, addressing critical challenges in vehicle electrification.

5.1. Topology Optimal Bracket CAD Model Parameterization

For the bracket design problem, the objective is to minimize the bracket's weight while maintaining stiffness constraints. Modifications were made to the existing topology optimization code to achieve this. The revised TO code is in the Appendix G. The $v_{fraction}$ was changed to be the objective of the function when compliance is one of the constraints. Using the same compliance as the default topology optimization result, the minimum volume fraction was reduced from 0.7 to 0.63 in the modified code, as shown in Table 8. However, this adjustment resulted in a large checkerboard pattern due to the low filter radius. The filter radius, *rmin,* was increased to 1.2 to address this issue and improve the structure while maintaining a 0.63 volume fraction as the input. This refinement produced a clearer structural pattern, with the compliance increasing from 219 to 232, as shown in the final column.

Table 8 Optimal Volume Fraction Results

Element size 66x22	Rectangular	Default TO	HPO-TO	Final Design
p	3	3	2	2
r_{min}	1.5	1.5	1	1.2
compliance	181.4778	219.5302	219	232
Volume Fraction	1	0.7	0.63	0.63
Optimized structure				

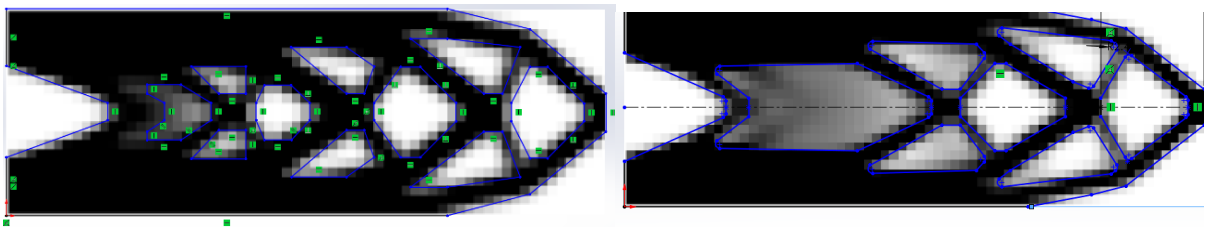

Figure 38 Sketch of the Structure from the Default TO (left) and Final Design (right)

To validate the stiffness of the optimized structure after HPO and compare it to the default algorithm results, CAD models were generated to serve as the geometry for static and fatigue FEA in ANSYS.

A sketch of the CAD model parameterization is depicted in Figure 36. The topology optimization results were scaled to dimensions of 330 x 110 mm, serving as a side-view reference on the background in SolidWorks via the Sketch Picture function. The sketch line was aligned with the grey elements along the edges. During the sketching process of the final design, a large, blurred area and an incomplete structure were observed, as shown in Figure 38. This section was considered void, with only the significant black elements deemed solid. CAD models of design from default TO and HPO-TO are shown in Appendix H.

5.2. FEA Results Analysis and Comparison

The ANSYS FEA results in Table 9 demonstrate that the optimal hyperparameters achieved a 48% weight reduction compared to the original rectangular plate, with an additional 13% reduction over the design from default topology optimization. The static safety factor decreased from 2.52 to 2.18 with the increased maximum Von-Mises stress. Despite this reduction, no fatigue damage was observed in the fatigue analysis, confirming the design's acceptability. Furthermore, these results validate that increasing r_{min} from 1 to 1.2 sacrifices some stiffness but effectively expands the filter area, averaging the distributed element density and mitigating checkerboard issues.

Table 9 FEA Results Comparison

Element size 66x22	Rectangle	default TO	Final Design
Max Von-Mises stress (Pa)	6.08E+07	1.30E+08	1.51E+08
Safety Factor	5.399	2.518	2.1758
Fatigue Safety Factor	3.575	1.667	1.4404
Weight (kg)	3.703284	2.384772	1.919892
Weight Reduction (%)		35.60%	48.15%

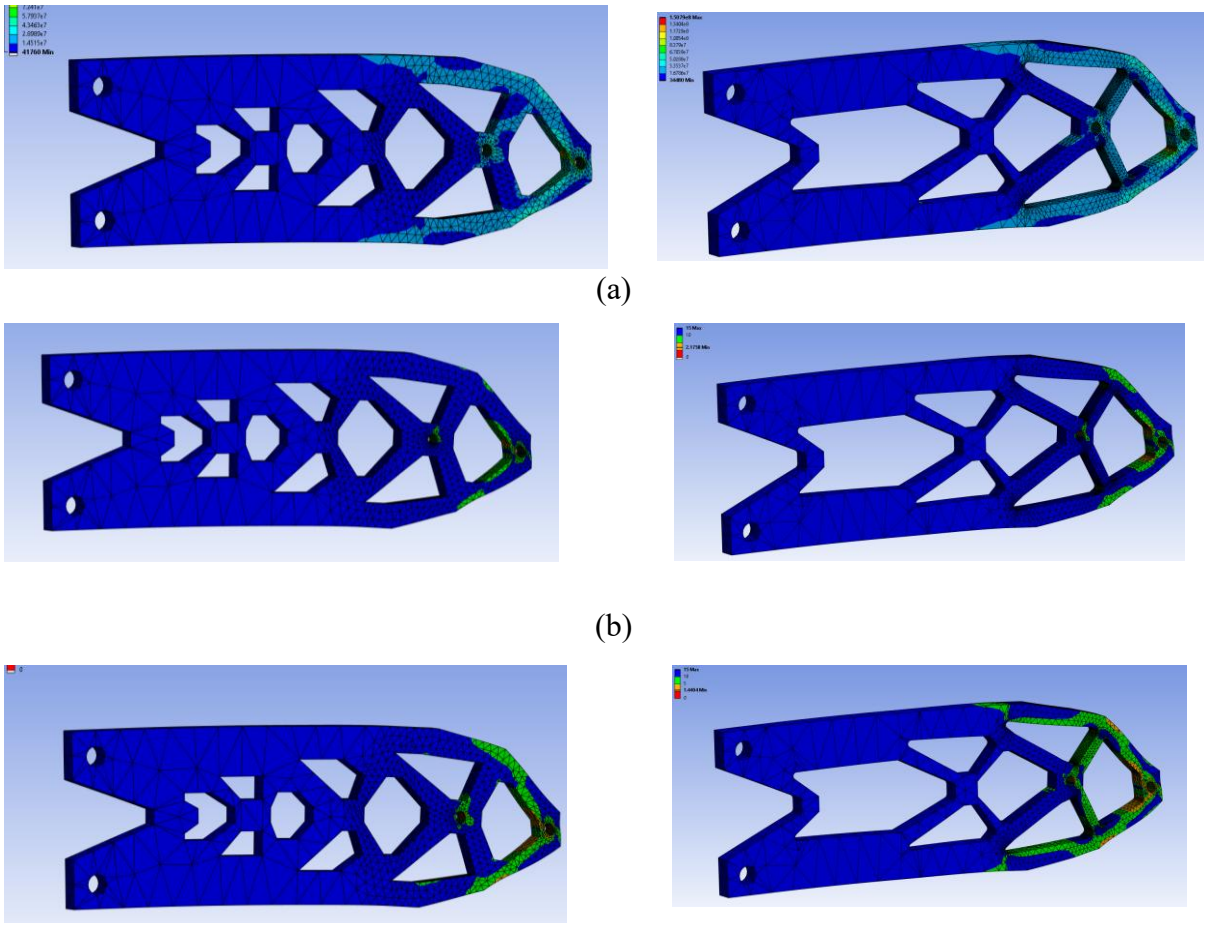

a): Max Von-Mises Stress b): Stress Safety Factor c): Fatigue Safety Factor

Figure 39 Comparison between the Design from Default TO (left) and Final Design (right)

This topology design optimization on the motor mounting bracket showed the huge potential for truck structure weight-reducing design improvements. The same principle and process can be applied to many heavy components of the e-MDT. This study explored the feasibility and benefit of part topology design optimization. Future studies on more truck structure components can be carried out.

6. Conclusion

This report demonstrates the successful design and optimization of key components for an electric medium-duty truck (e-MDT) retrofitted from a Toyota Dyna. The optimized powertrain layout effectively balances spatial constraints, weight distribution, and safety requirements while meeting vehicle dynamics and regulatory standards. Through reverse engineering and advanced simulation techniques, the integration of components was carefully planned to ensure compatibility with the existing chassis.

The structural redesign and analysis of critical components, such as the gearbox mounting bracket and frame, confirmed their adequacy under static and dynamic loads. Finite element analysis validated the designs, ensuring they meet performance criteria under operational conditions. Furthermore, applying topology optimization combined with hyperparameter tuning enabled a significant 48% weight reduction in the motor bracket, enhancing payload capacity without compromising structural integrity.

This work highlights the feasibility of adapting conventional vehicle platforms for electrification using modern engineering and optimization methodologies. By addressing challenges in layout design, structural analysis, and weight reduction, the project contributes to advancing sustainable transportation solutions. The approach and findings provide a solid foundation for future research, including exploring alternative materials, improving energy efficiency, and refining manufacturing processes to optimize electric vehicle designs further.

While the weight reduction achieved in the bracket design is technically significant, its impact on the overall truck design is minimal, contributing to less than 0.4% of the total vehicle weight. However, the topology optimization methodology remains highly relevant for electric vehicle (EV) design, as EVs are inherently heavier than their internal combustion engine (ICE) counterparts. Applying similar optimization techniques to more substantial components, such as the truck's ladder frame, could yield more impactful results.

Future work should explore topology optimization for the ladder frame, where significant weight savings could enhance vehicle efficiency and performance. However, this presents major challenges, including the complexity of multi-directional loading conditions and the significantly larger mesh sizes required for accurate finite element analysis. These factors introduce greater computational demands, making the problem more intricate and requiring advanced optimization algorithms and high-performance computing resources. Addressing these challenges could lead to meaningful advancements in lightweight and structurally efficient EV chassis designs.

References

[1] U.S. Environmental Protection Agency (EPA), *Greenhouse Gas Emissions Standards for Heavy-Duty Vehicles-Phase 3*. Washington, D.C., 2023. Accessed: Feb. 04, 2025. [Online]. Available: https://www.epa.gov/regulations-emissions-vehicles-and-engines/final-rule-greenhouse-gas-emissions-standards-heavy-duty

[2] The European Parliament and the Council of the Union, "Regulation (EU) 2019/1242 of the European Parliament and of the Council," *Official Journal of the European Union*, no. L198, pp. 202–240, Jul. 2019, Accessed: Feb. 04, 2025. [Online]. Available: http://data.europa.eu/eli/reg/2019/1242/oj

[3] L. Yang and H. He, "China's Stage VI Emission Standard for Heavy-Duty Vehicles (FINAL RULE)," 2018. Accessed: Feb. 04, 2025. [Online]. Available: https://theicct.org/publication/chinas-stage-vi-emissions-standard-for-heavy-duty-vehicles-final-rule/

[4] S. Mao and F. Rodriguez, "The Evolution of Heavy-duty Vehicles in China: A retrospective evaluation of CO 2 and pollutant emissions from 2012 to 2021," 2022. Accessed: Feb. 04, 2025. [Online]. Available: https://theicct.org/publication/china-hvs-ndc-tia-evolution-hdv-emissions-oct22/

[5] G. Kalghatgi, "Is It Really the End of Internal Combustion Engines and Petroleum in Transport?," *Appl Energy*, vol. 225, pp. 965–974, Sep. 2018, doi: 10.1016/j.apenergy.2018.05.076.

[6] F.J.R. Verbruggen, V. Rangarajan, and T. Hofman, "Powertrain Design Optimization for a Battery Electric Heavy-duty Truck," in *2019 American Control Conference (ACC)*, Philadelphia, PA, USA, 2019, pp. 1–6. doi: 10.23919/ACC.2019.8814771.

[7] Mullen Commercial, "Mullen THREE Owner's Manual," 2024. Accessed: Feb. 04, 2025. [Online]. Available: https://www.mullenusa.com/mullen-vehicle-center

[8] GreenPower Motor Company, "EV Star Truck Specification." Accessed: Feb. 04, 2025. [Online]. Available: https://greenpowermotor.com/gp-products/ev-star-cc/

[9] R. M. Salgado, F. Danzi, J. E. Oliveira, A. El-Azab, P. P. Camanho, and M. H. Braga, "The Latest Trends in Electric Vehicles Batteries," *Molecules*, vol. 26, no. 11, Jun. 2021, doi: 10.3390/molecules26113188.

[10] Y. Miao, P. Hynan, A. Von Jouanne, and A. Yokochi, "Current Li-ion Battery Technologies in Electric Vehicles and Opportunities for Advancements," *Energies (Basel)*, vol. 12, no. 6, p. 1074, Mar. 2019, doi: 10.3390/en12061074.

[11] M. A. Hannan, M. M. Hoque, A. Hussain, Y. Yusof, and P. J. Ker, "State-of-the-Art and Energy Management System of Lithium-Ion Batteries in Electric Vehicle Applications: Issues and Recommendations," Mar. 20, 2018, *Institute of Electrical and Electronics Engineers Inc.* doi: 10.1109/ACCESS.2018.2817655.

[12] M. Fichtner, "Recent Research and Progress in Batteries for Electric Vehicles," *Batter Supercaps*, vol. 5, no. 2, p. e202100224, 2022, doi: 10.1002/batt.202100224.

[13] H. A. Gabbar, A. M. Othman, and M. R. Abdussami, "Review of Battery Management Systems (BMS) Development and Industrial Standards," *Technologies (Basel)*, vol. 9, no. 2, p. 28, Jun. 2021, doi: 10.3390/technologies9020028.

[14] Toyota Motor Corporation, *Toyota Dyna Truck Body-builder Manual* . Japan, 2001. Accessed: Feb. 04, 2025. [Online]. Available: https://www.toyota-tech.eu/BBG/Dyna%20BBG%20BBGU-CD001/cont/pdf/BBGU2105.pdf

[15] Toyota Motor Corporation, *Toyota Dyna Fire Truck 1999 Body Builder's Guide*. Japan, 1999. Accessed: Feb. 04, 2025. [Online]. Available: https://www.toyota-tech.eu/BBG/Dyna%20BBG%20BBGU-CD001-1/BBGU1004.pdf

[16] T. Tang *et al.*, "Topology Optimization: A Review for Structural Designs Under Statics Problems," *Materials*, vol. 17, no. 23, p. 5970, Dec. 2024, doi: 10.3390/ma17235970.

[17] D. Jankovics and A. Barari, "Customization of Automotive Structural Components using Additive Manufacturing and Topology Optimization," in *IFAC-PapersOnLine*, Elsevier B.V., 2019, pp. 212–217. doi: 10.1016/j.ifacol.2019.10.066.

[18] J. H. Zhu, W. H. Zhang, and L. Xia, "Topology Optimization in Aircraft and Aerospace Structures Design," *Archives of Computational Methods in Engineering*, vol. 23, no. 4, pp. 595–622, Dec. 2016, doi: 10.1007/s11831-015-9151-2.

[19] J. Park, D. Lee, and A. Sutradhar, "Topology Optimization of Fixed Complete Denture Framework," *Int J Numer Method Biomed Eng*, vol. 35, no. 6, Jun. 2019, doi: 10.1002/cnm.3193.

[20] L. Mei and Q. Wang, "Structural Optimization in Civil Engineering: A literature Review," Feb. 2021, *Buildings*. doi: 10.3390/buildings11020066.

[21] M. P. Bendsoe, "Optimal Shape Design as a Material Distribution Problem," *Structural Optimization*, vol. 1, pp. 193–202, 1989, doi: 10.1007/BF01650949.

[22] G. I. N. Rozvany, M. Zhou, and T. Birker, "Structur OptimiTation Generalized Shape Optimization without Homogenization," *Structural Optimization*, vol. 4, pp. 250–252, 1992, doi: 10.1007/BF01742754.

[23] O. Sigmund, “A 99 Line Topology Optimization Code Written in MATLAB,” *Structural and Multidisciplinary Optimization*, vol. 21, no. 2, pp. 120–127, 2001, doi: 10.1007/s001580050176.

[24] B. Bischl *et al.*, “Hyperparameter Optimization: Foundations, Algorithms, Best Practices and Open Challenges,” 2021. Accessed: Feb. 04, 2025. [Online]. Available: https://arxiv.org/abs/2107.05847

[25] M. Ogunsanya, J. Isichei, and S. Desai, “Grid Search Hyperparameter Tuning in Additive Manufacturing Processes,” *Manuf Lett*, vol. 35, pp. 1031–1042, 2023, doi: 10.1016/j.mfglet.2023.08.056.

[26] J. Bergstra, J. B. Ca, and Y. B. Ca, “Random Search for Hyper-Parameter Optimization Yoshua Bengio,” *Journal of Machine Learning Research*, vol. 13, no. 2, pp. 281–305, 2012, doi: 10.5555/2188385.2188395.

[27] J. Snoek, H. Larochelle, and R. P. Adams, “Practical Bayesian Optimization of Machine Learning Algorithms,” in *Advances in Neural Information Processing Systems 25*, 2012. Accessed: Feb. 04, 2025. [Online]. Available: https://papers.nips.cc/paper/4522-practical-bayesian-optimization-of-machine-learning-algorithms

[28] L. Yang and A. Shami, “On Hyperparameter Optimization of Machine Learning Algorithms: Theory and Practice,” *Neurocomputing*, vol. 415, pp. 295–316, Nov. 2020, doi: 10.1016/j.neucom.2020.07.061.

[29] G. A. Lujan-Moreno, P. R. Howard, O. G. Rojas, and D. C. Montgomery, “Design of Experiments and Response Surface Methodology to Tune Machine Learning Hyperparameters, with a Random Forest Case-study,” *Expert Syst Appl*, vol. 109, pp. 195–205, Nov. 2018, doi: 10.1016/j.eswa.2018.05.024.

Appendices

6.1. Appendix A: Toyota Dyna Dyna Frame and Cabin Geometry

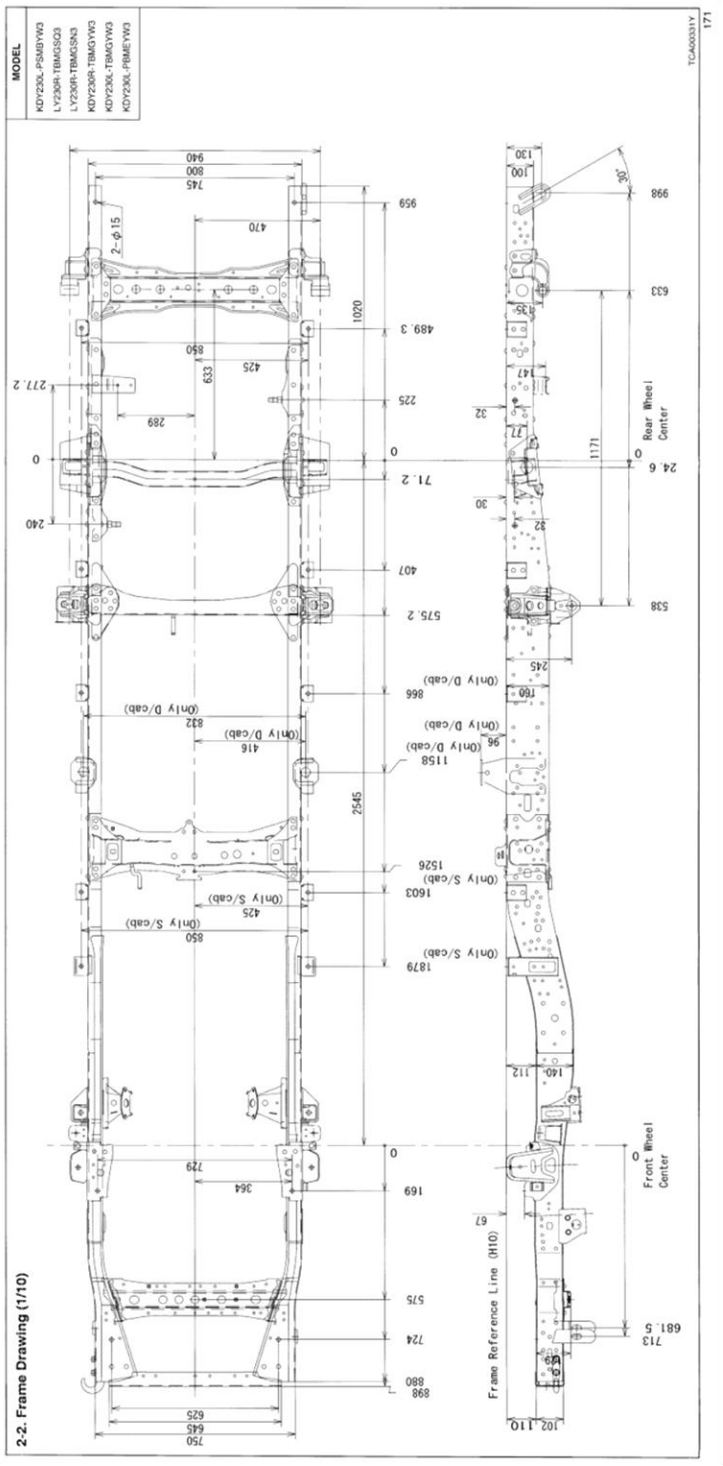

Figure 40: 2-D Drawing of Dyna Frame

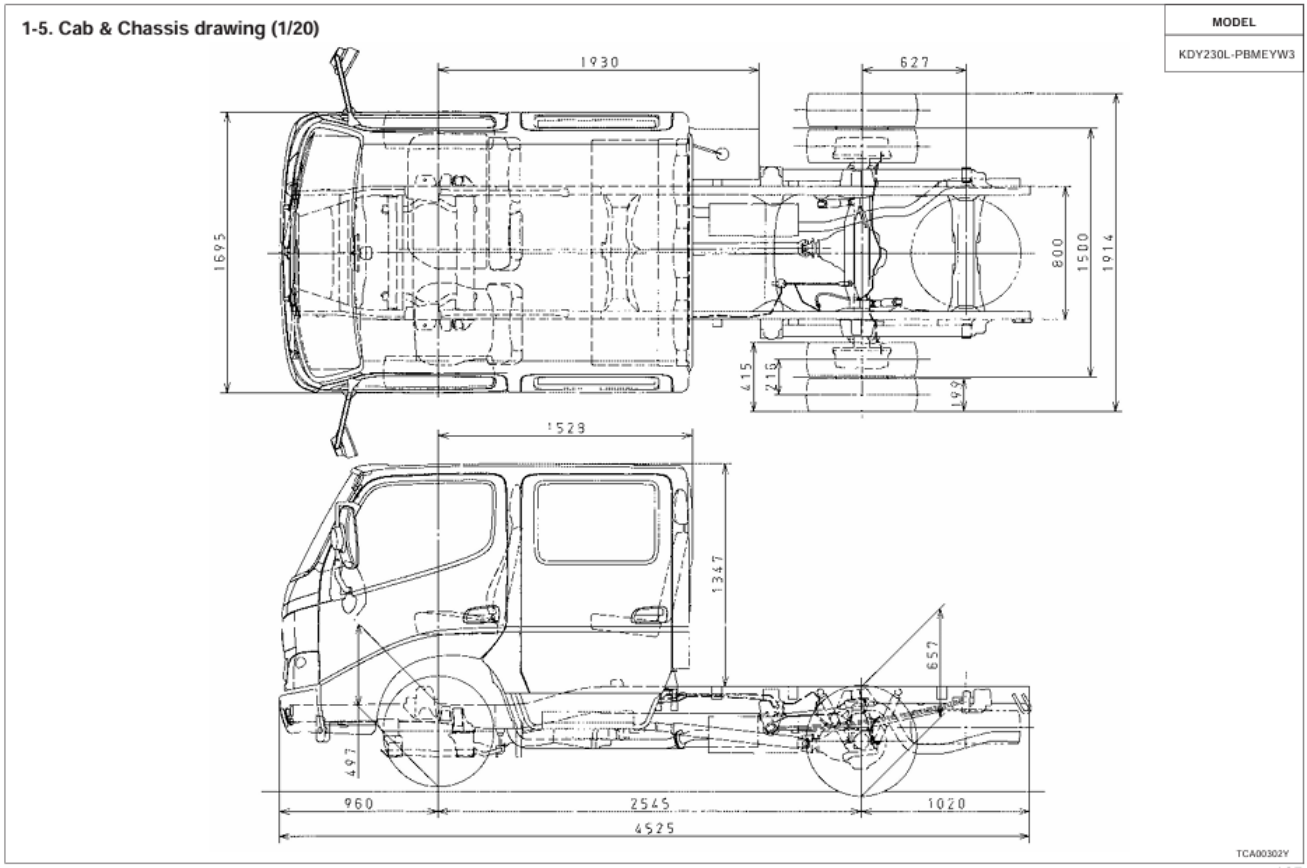

Figure 41: 2-D Drawing of Dyna Chassis

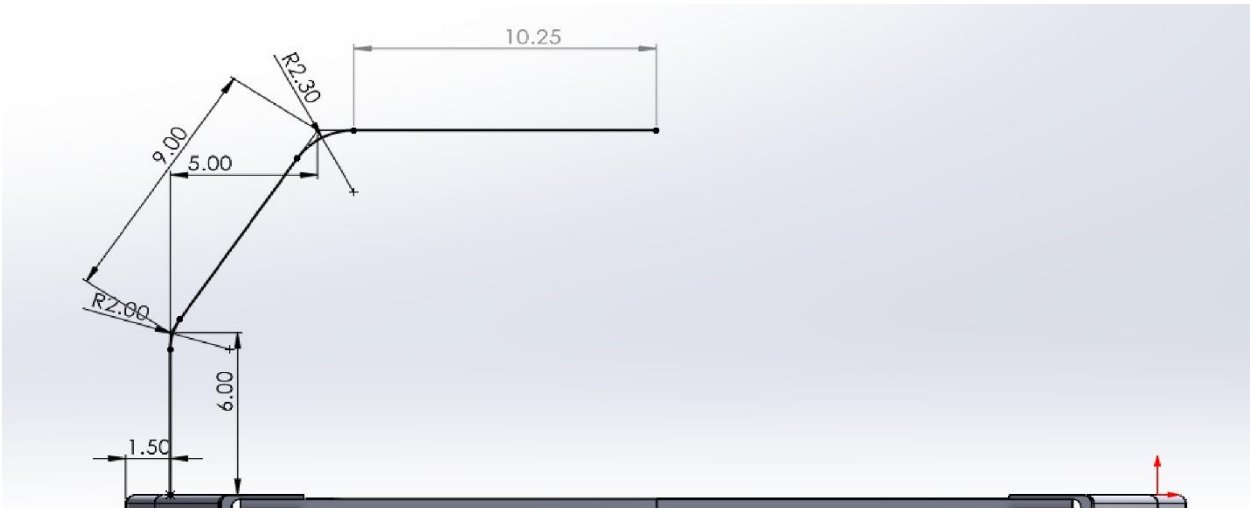

Figure 42: Cross-bar under the Cab Dimension Measurement

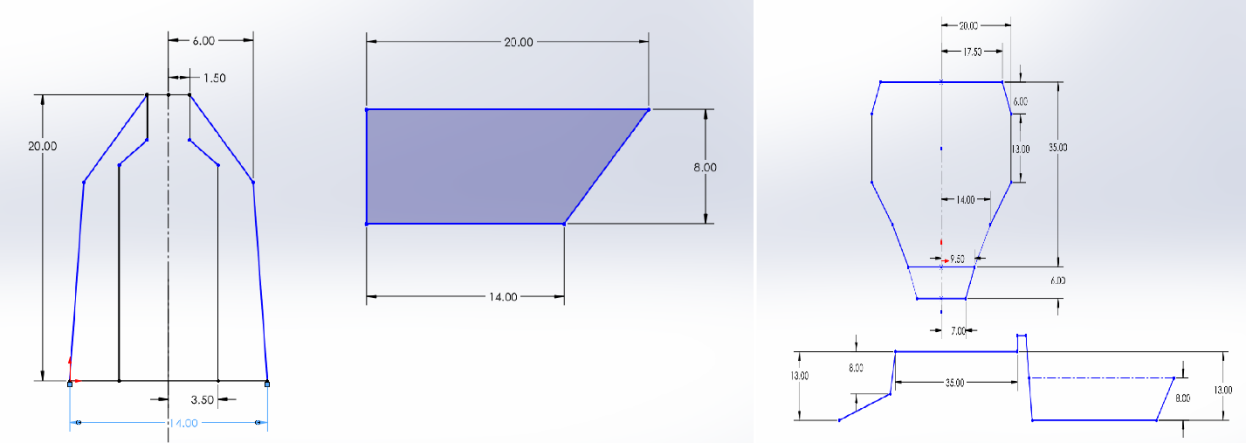

Figure 43: Cab under Surface Dimension Measurement (Manually)

6.2. Appendix B: Bolt Size Calculation for Gearbox and Motor Mount

```
Mass = 102;  % total mass
% Mass=58.1; %[kg] mass distributed on motor
% Mass=43.9; %     mass distributed on Gb[kg]
% maxLateralDecel=20*9.81; %[m/s^2] Considering 20G deceleration
maxVerticalAcc=3*9.81;     %[m/s^2] Considering 3G vertical acceleration
% maxLateralForce=maxLateralDecel*Mass %[N]
maxVerticalForce=maxVerticalAcc*Mass;

boltUltimateTensileImperial=150000; %[psi] Using Grade 8 bolts for automotive

boltUltimateTensileMetric=boltUltimateTensileImperial/145; %[MPa]

boltShearStrength=boltUltimateTensileMetric*0.6 %[MPa]

numBolts=3;% for crossbar to mounting plate
% numBolts=8;% whole assembly
SF=5;
% maxSheerStress=maxLateralForce*SF/numBolts;
maxSheerStress=maxVerticalForce*SF/numBolts;
boltDiameterMetric=sqrt((4*maxSheerStress)/(pi*boltShearStrength)) %[mm]
boltDiameterInch=boltDiameterMetric/25.4

% BoltDiameterMetric = 5.0653 mm holes between frame&crossbar
% BoltDiameterMetric = 3.2036 mm holes between plate&crossbar
```

6.3. Appendix C: Gearbox and Motor COG Calculation

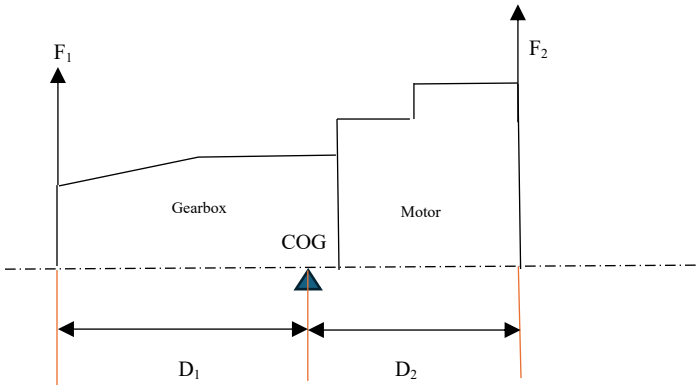

Figure 44 Gearbox and Motor COG Calculation

$$M_0 = M_G + M_m = 38 + 64 = 102kg$$

$$F_1 D_1 = F_2 D_2$$

$$F_1 + F_2 = M_0 g$$

$$D_1 = 291.68mm$$

$$D_2 = 220.44mm$$

$$g = 9.8\ m/s^2$$

Solve for

$$F_1 = 439.0\ N$$

$$F_2 = 581.2N$$

M_G is the mass of the gearbox. M_m is the mass of the motor. F_1 is defined as the total force from brackets on the gearbox side. F_2 is defined as the total force from brackets on the motor side. D_1 and D_2 is determined by the assembly CAD model of the gearbox and motor. Figure 44 shows the side view 2-D profile of the assembly.

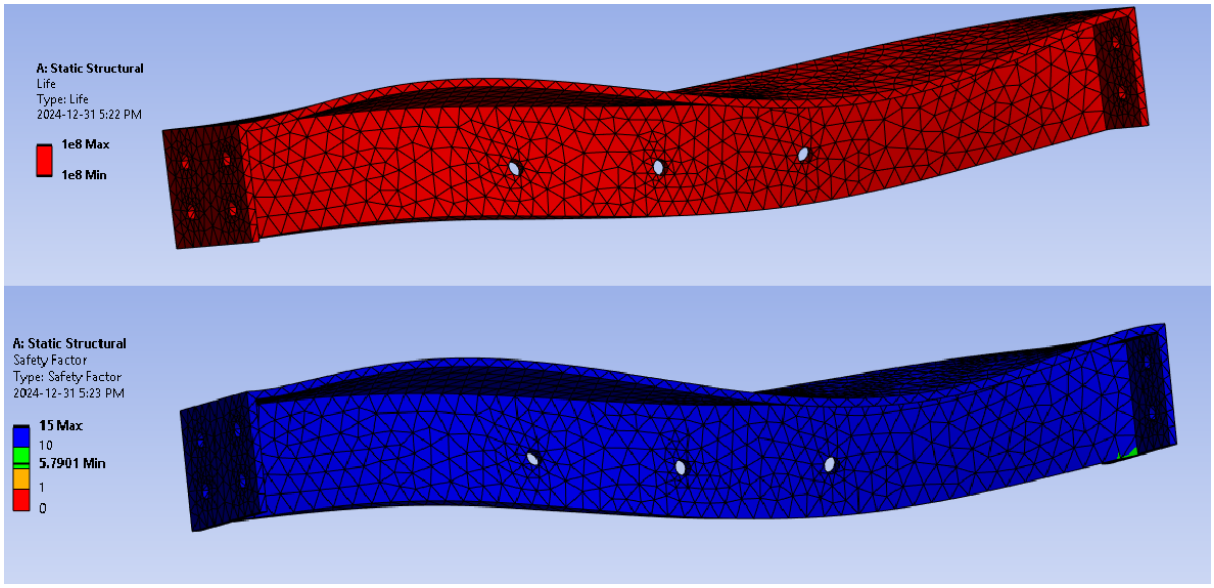

Figure 45: Fatigue Life (top) and Factor of Safety (bottom) of Gearbox Crossbar

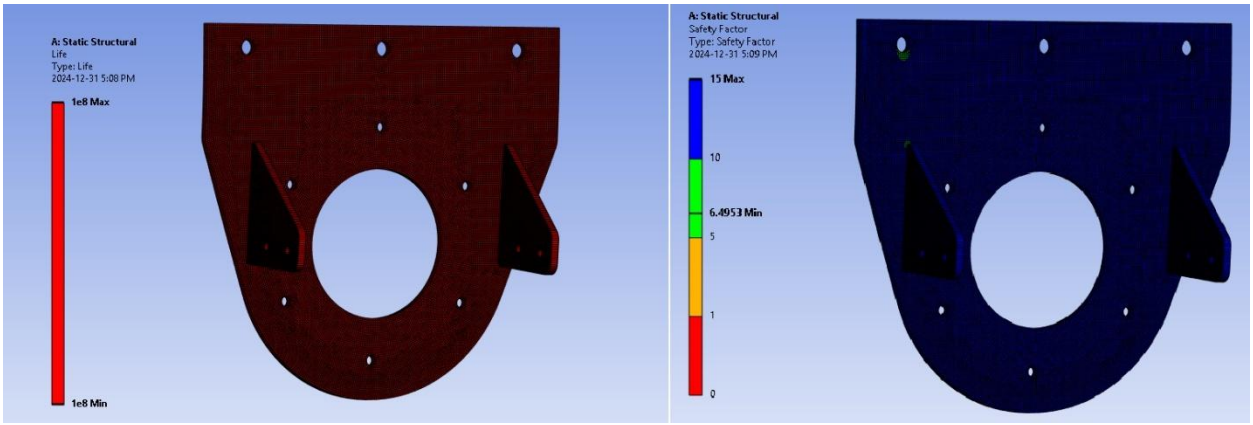

Figure 46: Fatigue life (left) and safety factor (Right) of Gearbox Mounting Plate

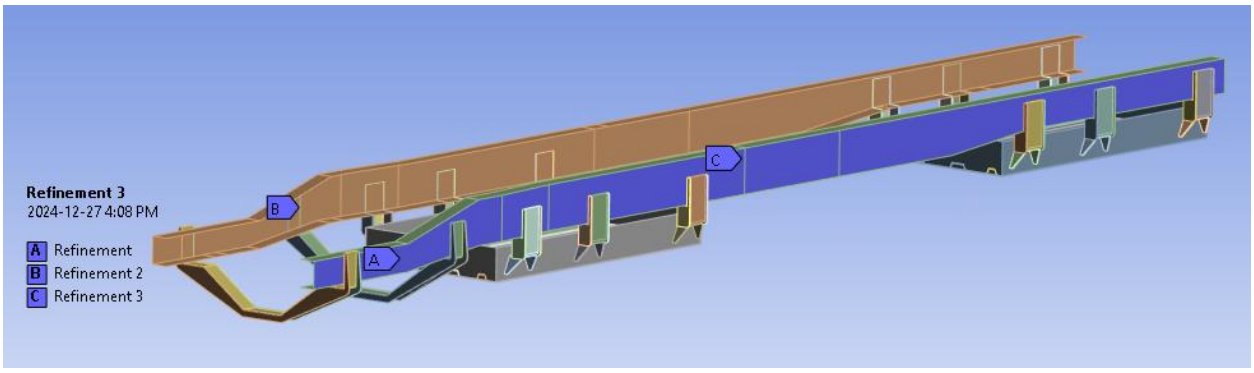

Figure 47: Mesh Refinement Area

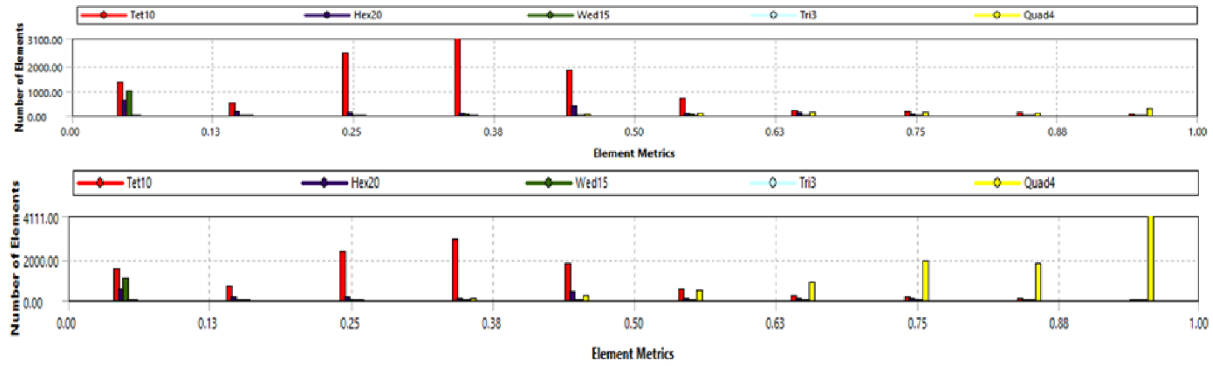

Figure 48: Default Element Metrics (Top) and Refined Element Metrics (Bottom)

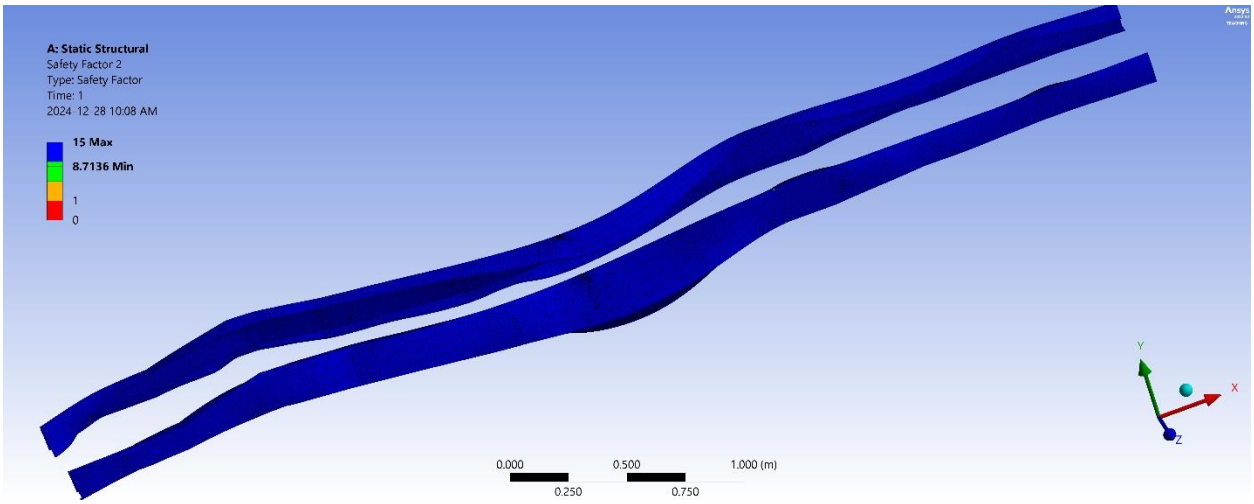

Figure 49: Frame Fatigue Analysis Safety Factor

6.4. Appendix D: Hyperparameter Optimization Codes

```
designPoints = bbdesign(3); % Matlab function to generate the 3 variables level Box-Behnken
design;

%Use short format for display
format short g

%create the dataset
design = dataset({designPoints, 'p','rmin','volfrac'});
bounds = [2 4; 1 2; 0.5 0.7];                          % limits for each variable
designBounds = dataset({bounds', 'p',' rmin', 'volfrac'});

%replace the normalized variables from the BB design with the actual design
%values

design.p = interp1([-1,1],designBounds.p, design.p);
design.rmin = interp1([-1,1],designBounds.rmin, design.rmin);
design.volfrac = interp1([-1,1],designBounds.volfrac, design.volfrac);

%Plot of the design space to be tested
sampleplot(bounds, design);

% %Generate data from experiments; Using parameters in design matrix to to
% run 2 load TO and get the final compliance
% output it to an Excel File

regData = xlsread('test(response).xlsx');  % read the data from the Excel sheet

% The form of our quadratic model:
%
%    AF = B0 + B1*h + B2*w + B3*t + B4*h*w + B5*h*t + B6*w*t + B7*h^2 + B8*w^2 + B9*t^2
%

sModel = regstats(regData(:,4), regData(:,1:3), 'quadratic');
rsquare = sModel.rsquare;
fprintf('\nThe R-square value is %g\n', rsquare)

seeResponse(sModel, designBounds);

rstool(regData(:,1:3), regData(:,4),'quadratic', 0.05, ...
  {'p', 'rmin', 'volfrac'}, 'compliance');

[optimVal,fval,exitflag,output,lambda,grad,hessian] = optimizeC([2.5, 1.5,
0.55],bounds(:,1),bounds(:,2), sModel);
fprintf('\n\nOptimal Values:\n');
fprintf('  p: %7.6g mm\n' , optimVal(1));
fprintf('  rmin: %7.6g mm\n', optimVal(2));
fprintf('  Volfrac: %7.6g mm\n' , optimVal(3));

optDesign = dataset({optimVal, 'p','rmin','volfrac'});
optActual =  201.5395; %%%     Obtain by setting volfraction as 0.7, p = 2, rmin=1, run 2load TO
fprintf('\n\n The actual optimal function value is %7.6g . The difference is %7.6g
percent.\n\n',optActual, abs(fval-optActual)/optActual*100);
```

6.5. Appendix E: Hyperparameters Interaction Surface Plots

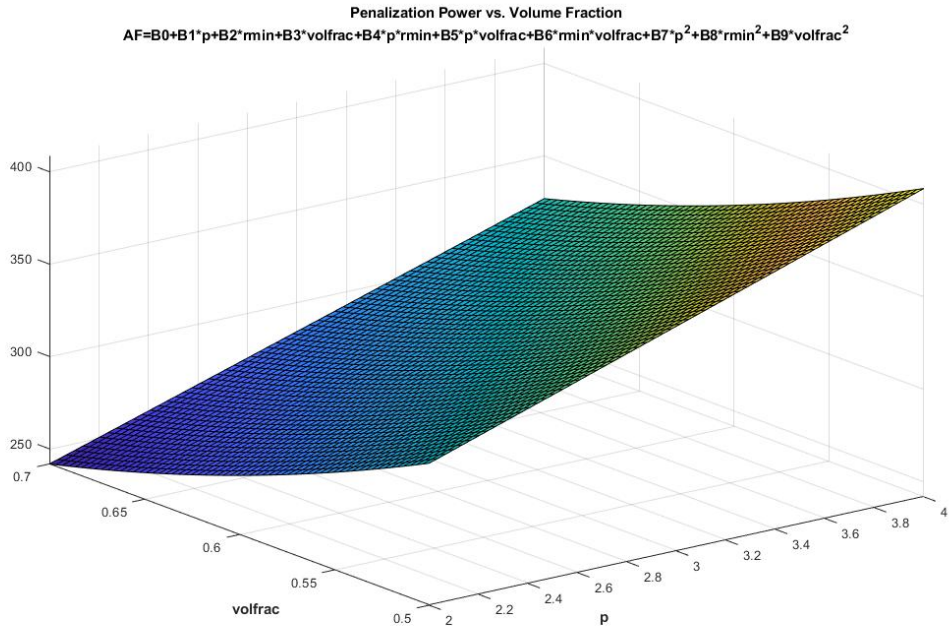

Figure 50 Response Surface: Penalization vs Volume Fraction

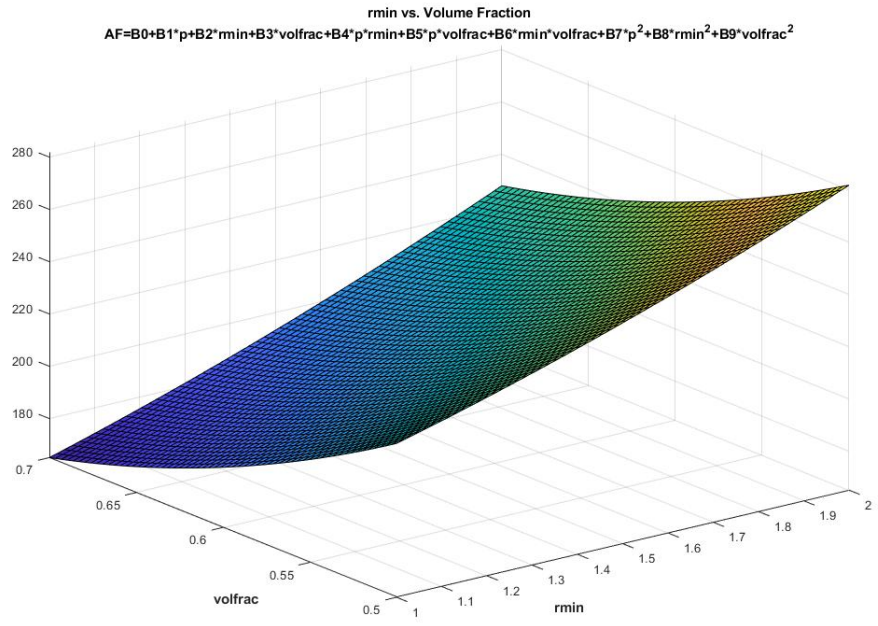

Figure 51 Response Surface: r_{min} vs Volume Fraction

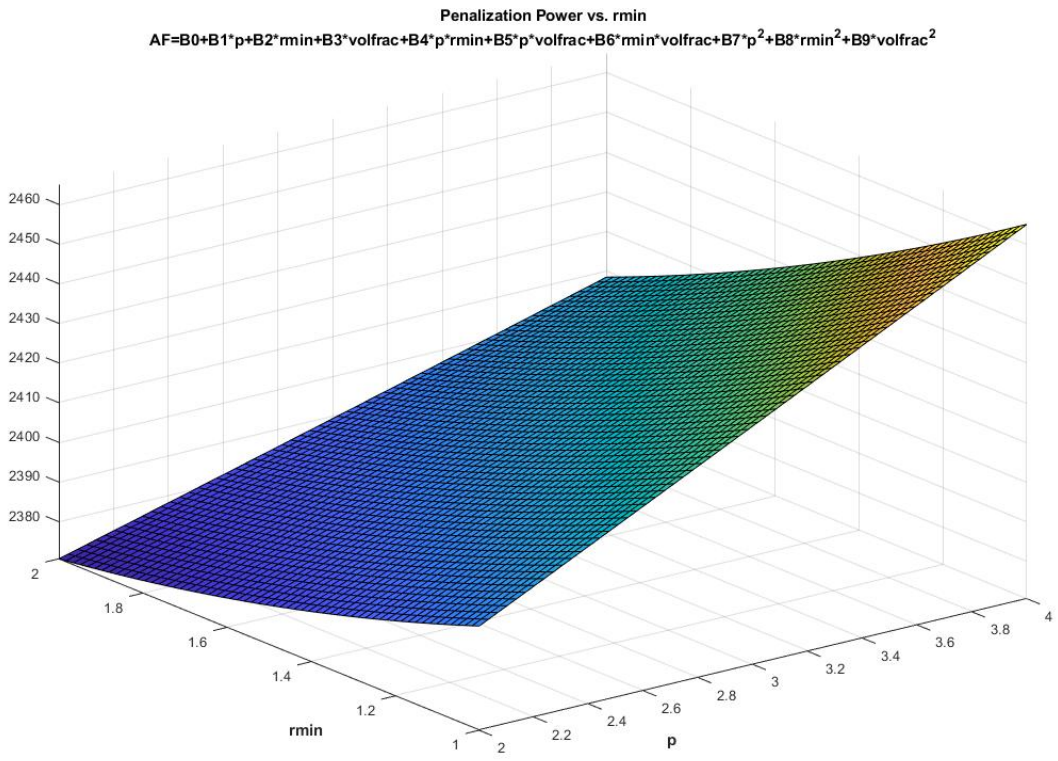

Figure 52 Response Surface: Penalization vs r_{min}

6.6. Appendix F: Modified TO Codes for Multi-load Scenario

```
% INITIALIZE
x(1:nely,1:nelx) = volfrac;
loop = 0;
change = 1.;
% START ITERATION
while change > 0.01
  loop = loop + 1;
  xold = x;
% FE-ANALYSIS
  [U]=FE(nelx,nely,x,penal);
% OBJECTIVE FUNCTION AND SENSITIVITY ANALYSIS
  [KE] = lk;
  c = 0.;
  for ely = 1:nely
    for elx = 1:nelx
      n1 = (nely+1)*(elx-1)+ely;
      n2 = (nely+1)* elx   +ely;
      dc(ely,elx) = 0.;
      for i = 1:2
      Ue = U([2*n1-1;2*n1; 2*n2-1;2*n2;2*n2+1;2*n2+2;2*n1+1;2*n1+2],i);
        c= c + x(ely,elx)^penal*Ue'*KE*Ue;
       dc(ely,elx) = dc(ely,elx)- penal*x(ely,elx)^(penal-1)*Ue'*KE*Ue;
      end
    end
  end
% FILTERING OF SENSITIVITIES
  [dc]   = check(nelx,nely,rmin,x,dc);
% DESIGN UPDATE BY THE OPTIMALITY CRITERIA METHOD
  [x]    = OC(nelx,nely,x,volfrac,dc);
% PRINT RESULTS
  change = max(max(abs(x-xold)));
  disp([' It.: ' sprintf('%4i',loop) ' Obj.: ' sprintf('%10.4f',c) ...
       ' Vol.: ' sprintf('%6.3f',sum(sum(x))/(nelx*nely)) ...
        ' ch.: ' sprintf('%6.3f',change )])
% PLOT DENSITIES
  colormap(gray); imagesc(-x); axis equal; axis tight; axis off;pause(1e-6);
end
%%%%%%%%%% OPTIMALITY CRITERIA
UPDATE %%%%%%%%%%%%%%%%%%%%%%%%%%%%%%%%%%%%%%%%%%%
```

```
function [xnew]=OC(nelx,nely,x,volfrac,dc)
l1 = 0; l2 = 100000; move = 0.1;
while (l2-l1 > 1e-4)
  lmid = 0.5*(l2+l1);
  xnew = max(0.001,max(x-move,min(1.,min(x+move,x.*sqrt(-dc./lmid)))));
  if sum(sum(xnew)) - volfrac*nelx*nely > 0
    l1 = lmid;
  else
    l2 = lmid;
  end
end
%%%%%%%%%% MESH-INDEPENDENCY
FILTER %%%%%%%%%%%%%%%%%%%%%%%%%%%%%%%%%%%%%%%%%%%%%%%%%%%%%%%%%%%%
function [dcn]=check(nelx,nely,rmin,x,dc)
dcn=zeros(nely,nelx);
for i = 1:nelx
  for j = 1:nely
    sum=0.0;
    for k = max(i-floor(rmin),1):min(i+floor(rmin),nelx)
      for l = max(j-floor(rmin),1):min(j+floor(rmin),nely)
        fac = rmin-sqrt((i-k)^2+(j-l)^2);
        sum = sum+max(0,fac);
        dcn(j,i) = dcn(j,i) + max(0,fac)*x(l,k)*dc(l,k);
      end
    end
    dcn(j,i) = dcn(j,i)/(x(j,i)*sum);
  end
end
%%%%%%%%%% FE-
ANALYSIS %%%%%%%%%%%%%%%%%%%%%%%%%%%%%%%%%%%%%%%%%%%%%%%%%%%%%%%%%%%%
%%%%%%%%%%%%%%
function [U]=FE(nelx,nely,x,penal)
[KE] = lk;
K = sparse(2*(nelx+1)*(nely+1), 2*(nelx+1)*(nely+1));
 F = sparse(2*(nely+1)*(nelx+1),2);
 U = sparse(2*(nely+1)*(nelx+1),2);
for elx = 1:nelx
  for ely = 1:nely
    n1 = (nely+1)*(elx-1)+ely;
    n2 = (nely+1)* elx   +ely;
```

```
    edof = [2*n1-1; 2*n1; 2*n2-1; 2*n2; 2*n2+1; 2*n2+2; 2*n1+1; 2*n1+2];
    K(edof,edof) = K(edof,edof) + x(ely,elx)^penal*KE;
  end
end
% DEFINE LOADS AND SUPPORTS (HALF MBB-BEAM)

F(2*(nely+1)*nelx+2*(nely/2+1),2) =-1;            % force on the middle of right edge
F(2*(nely+1)*(nelx*52/66+1)+2*(nely/2+1),1) = 1;   % force on the center

fixeddofs = [1:2*(nely+1)];                  % Left surface as fixed geometry
alldofs     = [1:2*(nely+1)*(nelx+1)];
freedofs    = setdiff(alldofs,fixeddofs);
% SOLVING
U(freedofs,:) = K(freedofs,freedofs) \ F(freedofs,:);
U(fixeddofs,:)= 0;
%%%%%%%%% ELEMENT STIFFNESS
MATRIX %%%%%%%%%%%%%%%%%%%%%%%%%%%%%%%%%%%%%%%%%%%%%%%%%%%%%%%%%%%%%%%%
function [KE]=lk
E = 1.;
nu = 0.3;
k=[ 1/2-nu/6   1/8+nu/8 -1/4-nu/12 -1/8+3*nu/8 ...
   -1/4+nu/12 -1/8-nu/8  nu/6       1/8-3*nu/8];
KE = E/(1-nu^2)*[ k(1) k(2) k(3) k(4) k(5) k(6) k(7) k(8)
                  k(2) k(1) k(8) k(7) k(6) k(5) k(4) k(3)
                  k(3) k(8) k(1) k(6) k(7) k(4) k(5) k(2)
                  k(4) k(7) k(6) k(1) k(8) k(3) k(2) k(5)
                  k(5) k(6) k(7) k(8) k(1) k(2) k(3) k(4)
                  k(6) k(5) k(4) k(3) k(2) k(1) k(8) k(7)
                  k(7) k(4) k(5) k(2) k(3) k(8) k(1) k(6)
                  k(8) k(3) k(2) k(5) k(4) k(7) k(6) k(1)];
```

6.7. Appendix F: Modified TO Code (*volfrac* as output)

```
% INITIALIZE
clear all
clc

volfrac = 0.7;    %% start initial volfrac and reduce volfrac 0.01 after each iteration
nelx = 66;        %% element mesh size: 5mm
```

```
nely = 22;
penal = 2;        % Optimal parameter from HPO
rmin = 1;
cf = 80;          % initial compliance, must smaller than compliance constraints
while cf< 219     % Default TO compliance  (2 load volfrac=0.7 p = 3 rmin = 1.5 )


x(1:nely,1:nelx) = volfrac;
loop = 0;
change = 1.;
% START ITERATION
while change > 0.01
  loop = loop + 1;
  xold = x;
% FE-ANALYSIS
  [U]=FE(nelx,nely,x,penal);
% OBJECTIVE FUNCTION AND SENSITIVITY ANALYSIS
  [KE] = lk;
  c = 0.;
  for ely = 1:nely
    for elx = 1:nelx
      n1 = (nely+1)*(elx-1)+ely;
      n2 = (nely+1)* elx    +ely;
      dc(ely,elx) = 0.;
      for i = 1:2
      Ue = U([2*n1-1;2*n1; 2*n2-1;2*n2;2*n2+1;2*n2+2;2*n1+1;2*n1+2],i);
        c= c + x(ely,elx)^penal*Ue'*KE*Ue;
       dc(ely,elx) = dc(ely,elx)- penal*x(ely,elx)^(penal-1)*Ue'*KE*Ue;
      end
    end
  end
% FILTERING OF SENSITIVITIES
  [dc]   = check(nelx,nely,rmin,x,dc);
% DESIGN UPDATE BY THE OPTIMALITY CRITERIA METHOD
  [x]    = OC(nelx,nely,x,volfrac,dc);
% PRINT RESULTS
  change = max(max(abs(x-xold)));
%   disp([' It.: ' sprintf('%4i',loop) ' Obj.: ' sprintf('%10.4f',c) ...
%        ' Vol.: ' sprintf('%6.3f',sum(sum(x))/(nelx*nely)) ...
%         ' ch.: ' sprintf('%6.3f',change )])
```

```
% % PLOT DENSITIES
%   colormap(gray); imagesc(-x); axis equal; axis tight; axis off;pause(1e-6);
end
  cf = c;
  volfrac = volfrac - 0.01;

end
%%%%%%%%%% OPTIMALITY CRITERIA
UPDATE %%%%%%%%%%%%%%%%%%%%%%%%%%%%%%%%%%%%%%%%%%%%%%%%%%%%%%%%%%%%
function [xnew]=OC(nelx,nely,x,volfrac,dc)
l1 = 0; l2 = 100000; move = 0.3;
 while (l2-l1 > 1e-4)
  lmid = 0.5*(l2+l1);
  xnew = max(0.001,max(x-move,min(1.,min(x+move,x.*sqrt(-dc./lmid)))));
  if sum(sum(xnew)) - volfrac*nelx*nely > 0;
    l1 = lmid;
  else
    l2 = lmid;
  end
 end
end
%%%%%%%%%% MESH-INDEPENDENCY
FILTER %%%%%%%%%%%%%%%%%%%%%%%%%%%%%%%%%%%%%%%%%%%%%%%%%%%%%%%%%%%%
function [dcn]=check(nelx,nely,rmin,x,dc)
dcn=zeros(nely,nelx);
 for i = 1:nelx
  for j = 1:nely
    sum=0.0;
    for k = max(i-floor(rmin),1):min(i+floor(rmin),nelx)
      for l = max(j-floor(rmin),1):min(j+floor(rmin),nely)
        fac = rmin-sqrt((i-k)^2+(j-l)^2);
        sum = sum+max(0,fac);
        dcn(j,i) = dcn(j,i) + max(0,fac)*x(l,k)*dc(l,k);
      end
    end
    dcn(j,i) = dcn(j,i)/(x(j,i)*sum);
  end
 end

end
```

```
%%%%%%%%%%% FE-
ANALYSIS %%%%%%%%%%%%%%%%%%%%%%%%%%%%%%%%%%%%%%%%%%%
%%%%%%%%%%%%%%
function [U]=FE(nelx,nely,x,penal)
[KE] = lk;
K = sparse(2*(nelx+1)*(nely+1), 2*(nelx+1)*(nely+1));
 F = sparse(2*(nely+1)*(nelx+1),2);
 U = sparse(2*(nely+1)*(nelx+1),2);
 for elx = 1:nelx
  for ely = 1:nely
    n1 = (nely+1)*(elx-1)+ely;
    n2 = (nely+1)* elx   +ely;
    edof = [2*n1-1; 2*n1; 2*n2-1; 2*n2; 2*n2+1; 2*n2+2; 2*n1+1; 2*n1+2];
    K(edof,edof) = K(edof,edof) + x(ely,elx)^penal*KE;
  end
 end

% DEFINE LOADS AND SUPPORTS (HALF MBB-BEAM)

F(2*(nely+1)*nelx+2*(nely/2+1),2) =-1;         % force on the middle of right edge
F(2*(nely+1)*(nelx*52/66+1)+2*(nely/2+1),1) = 1;   % force on the center
%fixeddofs   = union([1:2:2*(nely+1)],[2*(nelx+1)*(nely+1)]);
fixeddofs = [1:2*(nely+1)];
alldofs     = [1:2*(nely+1)*(nelx+1)];
freedofs    = setdiff(alldofs,fixeddofs);
% SOLVING
U(freedofs,:) = K(freedofs,freedofs) \ F(freedofs,:);
U(fixeddofs,:)= 0;
end
%%%%%%%%%%% ELEMENT STIFFNESS
MATRIX %%%%%%%%%%%%%%%%%%%%%%%%%%%%%%%%%%%%%%%%
function [KE]=lk
E = 1.;
nu = 0.3;
k=[ 1/2-nu/6   1/8+nu/8 -1/4-nu/12 -1/8+3*nu/8 ...
   -1/4+nu/12 -1/8-nu/8  nu/6       1/8-3*nu/8];
KE = E/(1-nu^2)*[ k(1) k(2) k(3) k(4) k(5) k(6) k(7) k(8)
                  k(2) k(1) k(8) k(7) k(6) k(5) k(4) k(3)
                  k(3) k(8) k(1) k(6) k(7) k(4) k(5) k(2)
                  k(4) k(7) k(6) k(1) k(8) k(3) k(2) k(5)
```

```
            k(5) k(6) k(7) k(8) k(1) k(2) k(3) k(4)
            k(6) k(5) k(4) k(3) k(2) k(1) k(8) k(7)
            k(7) k(4) k(5) k(2) k(3) k(8) k(1) k(6)
            k(8) k(3) k(2) k(5) k(4) k(7) k(6) k(1)];
end
```

6.8. Appendix H: CAD Models of Motor Mount Bracket Design

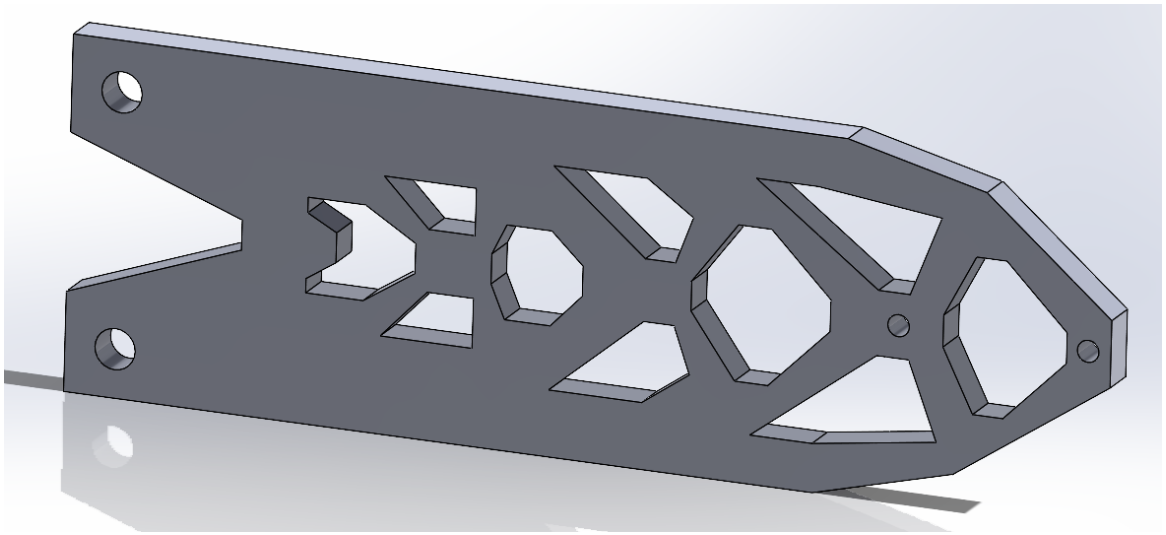

Figure 53 CAD Model of Design from Default TO

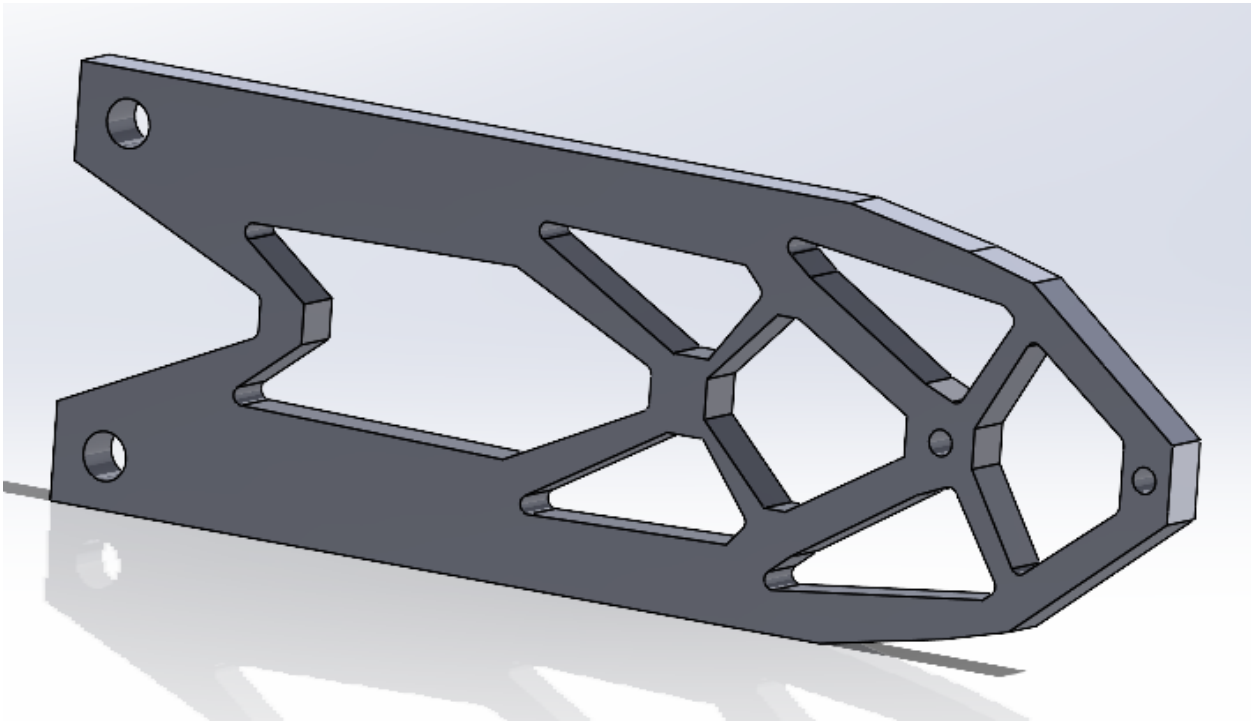

Figure 54 CAD Model of Design from HPO-TO